CHALMERS
UNIVERSITY OF TECHNOLOGY

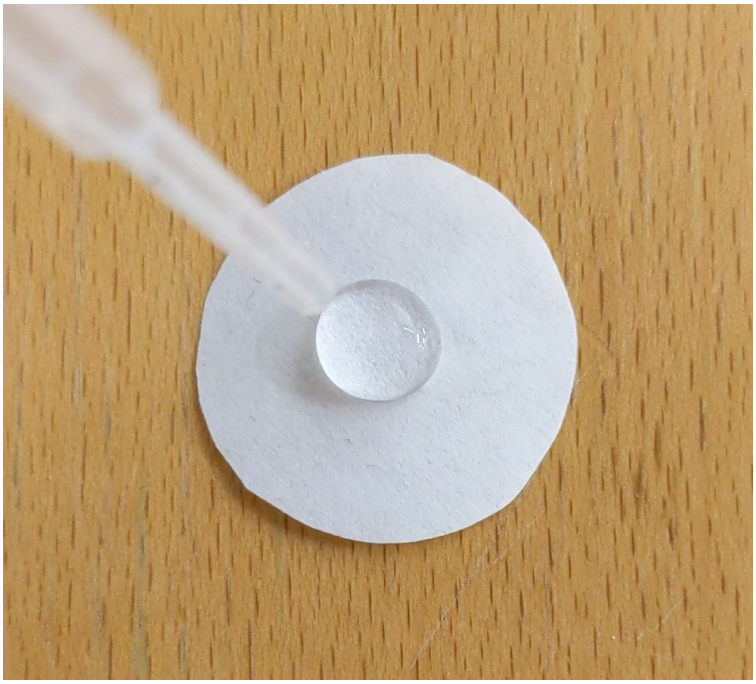

Monitoring Water Transport in Fiber-based Material

Master's thesis in Innovative and Sustainable Chemical Engineering

KHALID MOHAMED AND SHYAM KRISHNAN PISHARODY

DEPARTMENT OF CHEMISTRY AND CHEMICAL ENGINEERING
CHALMERS UNIVERSITY OF TECHNOLOGY
Gothenburg, Sweden 2023
www.chalmers.se

Master's thesis 2023

Monitoring Water Transport in Fiber-based Material

KHALID MOHAMED AND SHYAM KRISHNAN PISHARODY

CHALMERS
UNIVERSITY OF TECHNOLOGY

Department of Chemistry and Chemical Engineering
Division of Chemical Engineering
Chalmers University of Technology
Gothenburg, Sweden 2023

Monitoring Water Transport in Fiber-based Material

Khalid Mohamed and Shyam Krishnan Pisharody

Supervisors: Diana Bernin, Chalmers University
Maria Gunnarsson, Wellspect Healthcare
Åsa Westling, Wellspect Healthcare
Examiner: Diana Bernin, Department of Chemistry and Chemical Engineering

Master's Thesis 2023
Department of Chemistry and Chemical Engineering
Division of Chemical Engineering
Chalmers University of Technology
SE-412 96 Gothenburg
Telephone +46 31 772 1000

Cover: Placing of water droplets on paper sample.

Typeset in LaTeX
Gothenburg, Sweden 2023

Abstract

Knowledge of how a material absorbs water is crucial when selecting for packaging applications. In the case of clean intermittent catheters, the packaging is considered as a part of the medical device. These devices contain a sachet of liquid which is used to activate the hydrophilic catheter surface for comfortable use and to prevent complications in urethral health. This master thesis aims to investigate the water transport in fibre-based materials using the technique of Magnetic Resonance Imaging (MRI).

Initially, contact angle measurements and Cobb tests were done on the paper samples, provided by Wellspect Healthcare, to get a general idea about the wettability and hydrophobicity of the papers. Further, two MRI sequences were run on five different paper samples, with water on their surfaces, to understand more about the through-thickness water transport in them. A 1-D multiple-slice multiple-echo (MSME) sequence was run to get data on how the water signal intensity changes over time and across the thickness of the sample. Further, 2-D MSME sequences were run to correlate the image produced with the 1-D signal and verify the robustness of the method. Using these sequences, profiles of water signal intensity versus time were obtained for all papers. These profiles give a clear indication of the water absorption rates of these papers, which in turn helps in deciding which paper is suited best for the intended packaging application. Information about how long it takes for each paper to become saturated with water was also extracted. These results were also correlated with the contact angle and Cobb measurements.

FTIR spectroscopy was used to identify polymers coatings, if any, on the paper materials. The results obtained from the MRI sequences were then correlated with the findings from the FTIR. Further, the same experiments were repeated with 3 w/v% NaCl in distilled water. This salt solution is of significance as this is used to activate the catheter surface which then becomes isotonic, i.e, with the same osmotic pressure, to urine and hence ensures smooth and comfortable usage of the catheter.

In this study, it was determined that the samples AM SUP NL 60g and AM CRSTL 35 displayed a cellulose spectrum on both sides, leading to the assumption that they are non-treated. In contrast, the other three samples - WC gas paper 63 LC, AC grid paper KG 9411, and WC grid paper 70 - appeared to have been treated on one side.These treated samples have higher contact angles, suggesting the presence of hydrophobic treatments.The treatment was identified as ethylene/vinyl acetate co-polymer for WC gas paper 63 LC and a blend of polyethylene and polystyrene for AC grid paper KG 9411 and WC grid paper 70. WC gas paper 63 LC and AC grid paper KG 9411, in particular, showed high water resistance, marked by a contact angle greater than 90°, a Cobb value below 20 g/m^2, and a lower signal intensity

in MRI analysis.These properties make them more suitable for use as packaging material for this purpose than the other 3 samples.
Conversely, despite its treatment, WC grid paper 70 absorbed the highest amount of water, surpassing even the non-treated samples. This is assumed to be due insufficient coating thickness and inherent properties of the paper.

This work also gives an indication on how the method can be further optimized to extract better results from the MRI sequences.

Keywords: MRI, paper, water transport, hydrophobicity, signal intensity, saturation.

Acknowledgements

We take this opportunity to thank our supervisor and examiner from Chalmers University of Technology, Dr. Diana Bernin, for her guidance, enthusiasm and for inspiring us to be more curious throughout. We would also like to thank our supervisors from Wellspect Healthcare, Maria Gunnarsson and Åsa Westling, for being encouraging, approachable and for their support and advice during the course of the thesis.

We would like to thank Emmanouela Leventaki for her help with 3-D printing of parts required for our experiments. We would also like to thank Feryal Guerroudj and Saeed Khoshhal Salestan for their valuable advice and feedback during weekly meetings.

Finally, we would like to thank everyone at the Department of Chemistry and Chemical Engineering, Floor 2, for creating a great working environment and for helping out when we were in need.

List of Acronyms

Below is the list of acronyms that have been used throughout this thesis:

MRI	Magnetic Resonance Imaging
NMR	Nuclear Magnetic Resonance
MSME	Multiple Slice Multiple Echo
RF	Radio-frequency
TR	Repetition Time
TE	Echo Time
FOV	Field of View
SNR	Signal to Noise Ratio
N_{SA}	Number of Signal Averages
FTIR	Fourier Transform Infrared Spectroscopy
MD	Machine Direction
CD	Cross Direction
ZD	Through-thickness direction

Nomenclature

Below is the nomenclature of indices, sets, parameters, and variables that have been used throughout this thesis.

B	Magnetic Field
γ	Gyromagnetic ratio
ν	Larmor Frequency
T	Tesla

Contents

List of Figures

List of Tables

1

Introduction

1.1 Background

Packaging is an important aspect of healthcare devices fabrication because it protects the device to ensure that the device is clean and safe to use. For medical products, its packaging is also considered part of the product as it keeps it clean and safe to use. Plastic packaging is extensively used for this purpose. However, the growing problem of plastic pollution has prompted a search for alternative packaging materials. Plastic pollution is a growing concern because it accumulates in the environment and adversely affects wildlife, ecosystems, and human health. On the other hand, cellulose fibers, which are biodegradable and renewable, have already shown a great potential as a plastic packaging replacement.

Wellspect HealthCare is one of the most well known providers of devices for clean intermittent catheterization, and supplies catheters for both females and males under the brandname LoFric©. This product is currently contained in a plastic packaging along with a sachet of the liquid used to activate the hydrophilic coating on the catheter surface. It is recommended that self-catheterization is performed five times a day on average, which means that one product along with the packaging is discarded each time. These factors along with Wellspect's strong commitment towards creating sustainable and environmentally benign products, brought forth the idea to investigate the potential of fiber-based materials for the outer packaging of these medical devices.

Fundamental understanding about the properties and behavior of fiber-based materials, especially their ability to transport water, is critical for determining their suitability for intermittent catheter packaging. Water transport is an important aspect of catheter packaging because it affects the catheter's protection against the outer environment and the fluctuating relative humidity. In addition to this protection, the packaging is required to be resistant to water to a certain extent from the inside, as it also acts as a container for activation of the catheter surface. This is achieved through the release of a liquid upto 6 minutes before the device is used. Hence, it is important that the packaging would not leak the liquid for at least 30 minutes, to prevent spillage before, after or during use of the device.

This leads to the main challenge with paper materials. Paper materials have different properties, and most importantly, how water travels through it needs to be

understood. Fibers swell up when they come in contact with water, which can be prevented by functionalizing them with hydrophobic chemical groups within the material or on its surface. However, absorption of water cannot be fully avoided. Hence, it is of prime importance to study the water transport properties of such fiber-based materials.

1.2 Aim

The aim of this thesis is to increase the understanding of water transport properties in different types of paper fibers with the goal of finding a more environmentally friendly alternative to plastic packaging for potential use in clean intermittent catheterization packaging. Magnetic Resonance Imaging techniques are employed for this, using cellulose fibers treated to varying degrees and liquids of varying osmolalities.
The results of this study will hopefully assist to develop new types of catheter packaging materials that are efficient, safe, and more sustainable, minimizing the impact of plastic pollution on the environment.

2

Magnetic Resonance Imaging - MRI

2.1 Introduction to MRI

Magnetic Resonance Imaging or MRI, is an imaging technique that has been used traditionally in the medical field. It produces detailed images of body parts, without being invasive and hence is extremely useful for diagnosis. It has also found applications in detecting the water transport in paper materials [1]. Due to the spatial and temporal resolution it offers, it can be used to generate information on how water travels through the material during phenomena such as absorption or drying.
The MRI equipment consists of a magnet, a radio-frequency transmitter, receiver and magnetic field gradients. MRI is based on a concept called Nuclear Magnetic Resonance (NMR). It works on two principles; the effect of a magnetic field on the spin of nuclei and radio-frequency pulses to excite these nuclei. A brief description of the principles of NMR is given below [2].

- Atoms have three fundamental particles, electrons with a negative charge, protons with a positive charge and neutrons with neutral charge. Since the protons and neutrons are located inside the nucleus, all nuclei have positive charge. A property of the nucleus, which is of interest here, is its intrinsic spin.
- In the absence of a magnetic field, the individual spin orientations of all nuclei are randomly distributed and their vector sum is zero.
- When placed in an external magnetic field these nuclei will align themselves with the field and precess with a frequency ν, which is known as Larmor frequency. Precession can be better imagined as the rotation of the charged nuclei due to the magnetic field. The nuclei also spin in coherence with the other ones. This creates a net magnetization vector. The precession frequency is related to the magnetic field B, through the Larmor equation, which is given below.

  $$\nu = \gamma B \tag{2.1}$$

  where, γ is the gyromagnetic ratio, which is constant for each nucleus.
- Each nucleus can take two different energy levels. When aligned in the direction of the external magnetic field, it is at a low energy state, called spin up.

When aligned in the opposite direction, it is at a high energy state, called spin down. This is visualized in figure 2.1.

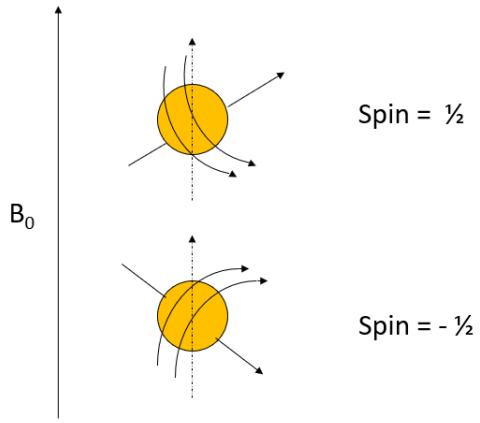

Figure 2.1: Two types of proton spin under a magnetic field

- The idea of magnetic resonance is to manipulate the net magnetization produced. This is done using short pulses of radio-frequency (RF) energy. This pulse is known as an RF-pulse.
- During the pulse, the nuclei in the nucleus absorb some of the energy at a specific frequency as described by equation 2.1. The spins are excited to be detected by the receiver.
- When the duration of the pulse ends, the nuclei come back to their original spin state. During this process, it emits a radio-frequency pulse which is detected by an RF receiver and converted to a signal.
- The signal is converted to intensity levels using Fourier-transform. The intensity levels in each pixel are displayed as different shades of gray colour which gives an image. The frequency of the RF pulse can be changed to get images with different contrast.
- In MRI, three gradient fields are produced by gradient coils and superimposed on the main magnetic field to help localizing the origin of signals [3]. These fields are slice selection gradient, the phase and frequency encoding gradients.
- The slice selection gradient is to determine slice position and thickness based on its variable magnetic field strength and the bandwidth of the radio frequency pulse. While the phase and frequency encoding gradients are applied perpendicularly to each other and the slice selection gradient to help determining the exact location from which the signal originates within a slice [3].
- These gradients are activated sequentially: slice selection with the RF pulse, phase encoding a bit after, and finally, frequency encoding during signal reception. The combined data is then processed to identify the exact point from which the signal is emitted [3].

2.2 Parameters for Imaging

There are two important parameters which can be changed to get images with different contrasts.

- **Echo Time (TE) :** This is the time which includes a 90° RF pulse, a subsequent 180° RF pulse before signal sampling. This parameter is related to an intrinsic property of the material which is called T_2 relaxation time, which is the time taken by the nuclei to lose coherence with the other nuclei. Changing TE can change the contrast with respect to T_2 relaxation time and hence produce T_2 weighted images.
- **Repetition Time (TR) :** This refers to the time between two consecutive scans during the imaging process. It is related to another intrinsic property called T_1 relaxation time, which is the time taken for the nuclei to re-align with the external magnetic field. Changing TR can result in contrast related to T_1 relaxation time and hence produce T_1 weighted images.

There are several more settings which can affect the image and the signal which are discussed below. To get a good signal, one needs to find the optimal combination of these settings.
Extraction of useful data from MRI results is often a difficult task due to poor signal-to-noise ratio. There are several more settings which can affect the image and signal. To get a good signal, one needs to find the optimal combination of these settings. These parameters and how they affect each other and the signal is discussed further.

- **Resolution** : Images generated by the MRI are composed of voxels, which represent one volume element in the image, similar to how pixels represent 2-D elements. The spatial resolution of the image is then dependant on the amount of information in each voxel. This depends on several factors such as size of the matrix, field of view (FOV), and slice thickness. Resolution is inversely proportional to voxel size and hence, more the number of voxels, better the resolution.

- **Field of View (FOV)** : This is usually measured in mm^2, and represents the total area from which MRI signals are sampled. Decreasing the FOV increases the spatial resolution by decreasing voxel size, while also decreasing the signal-to noise ratio (SNR).

- **Slice Thickness** : This is a parameter measured in mm, and it represents the volume, of the entity being imaged, that is available for excitation using RF pulses and subsequent production of signals. This volume is in the slice direction which is also set along with the slice thickness. Thicker slices mean more signal per voxel and hence better SNR.

- **Signal-To-Noise Ratio (SNR)** : Output from an MRI scan consists of both signal and noise. The ratio between these is defined as signal-to-noise ratio or SNR. It is a parameter used to describe the how good an MRI signal is.

- **Number of Signal Averages (N_{SA})** : It is the number of times the signal from one slice is measured and averaged. This is done in order to increase the SNR, however the scan time also increases. Doubling the N_{SA} increases the SNR by a factor of $\sqrt{2}$.

The important and common parameters to be optimized are the Repetition time, Echo time, Resolution, Slice thickness, FOV and N_{SA}. This is because, all of these settings affect the SNR of the signal from the MRI. How each of these settings affect the SNR is discussed below.

- Resolution : SNR is directly proportional to pixel size and hence is inversely proportional to resolution. There is an optimum range for the resolution, above which the images will be grainy due to lowered SNR and below which the images will be blurry due to increased SNR.
- Repetition Time : Higher TR allows for the longitudinal magnetization to get back to its maximum and hence give higher signal intensities. However, increasing it above a certain limit will decrease the effect of T1.
- Echo Time : A longer TE would result in the transverse magnetization going down which in turn would result in signal loss. Decreasing TE beyond a limit would reduce the T2 effect.
- FOV : SNR increases if the FOV is increased. Increased FOV results in increased pixel size which means more signal per pixel and hence increased SNR. However this reduces the spatial resolution.
- Slice Thickness : Increase in slice thickness increases SNR as the voxel size increases and there is more signal per voxel. However, this decreases the spatial resolution.
- N_{SA} : Increasing the number of averages would increase SNR since the data is acquired more times. However, this increases scan time. If FOV needs to be reduced, increasing N_{SA} can provide reasonable SNR.

3

Paper Materials and Water Transport

3.1 Paper Materials

Paper is a thin material produced from cellulose fibres extracted from wood or non-wood sources such as straw, bagasse and jute [4]. These sources contain biomass which is a complex structure composed of a network containing three major biopolymers called cellulose, hemicelluloses and lignin. In general, cellulose comprises of 40% to 50% of the wood cell chemical composition, while hemicelluloses make up 20% to 25% and lignin accounts for 25% to 30% [5]. On the microscopic level, these fibres can be observed as a matrix containing all three biopolymers. A schematic representation of the ultrastructure of a wood cellulose fibre is shown in figure 3.1.

Cellulose fibrils are oriented randomly in the primary cell wall while the secondary layer S1 has fibrils oriented almost horizontally and secondary layer S2 has them arranged almost vertically [5]. This orientation provides strength to the fibre. Hemicelluloses also contribute to the strength while acting as a connection between cellulose and lignin [6]. Lignin, which is highly present in the middle lamela, acts as a binder which holds together cellulose fibrils [5]. For production of paper from wood

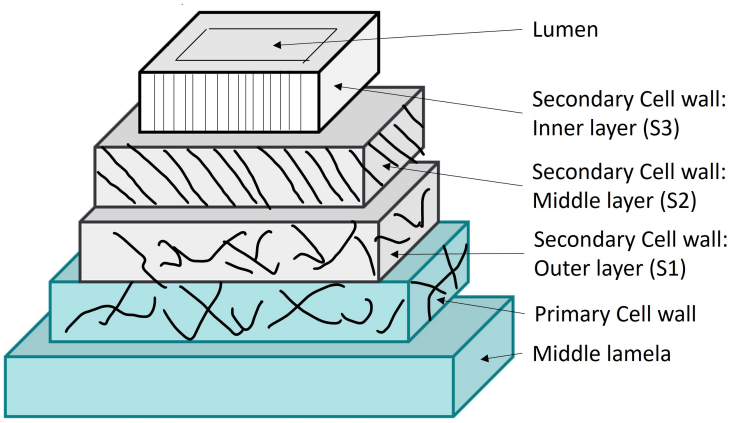

Figure 3.1: Different layers of a cellulose fibre ultrastructure

fibres, the fibres are liberated through a so-called pulping process. This can be either mechanical, where the fibres are taken out by grinding the wood chips or chemical, where cooking chemicals are used for de-lignification, i.e. removal of lignin to liberate fibres [7]. The common process used for this is called Kraft pulping, where a mixture of sodium hydroxide and sodium sulfide is used [8]. These fibres are then assembled using machines to form sheets of cellulose fibres called paper. Paper-making is a centuries-old process, with archaeological findings indicating its existence as early as 2nd Century B.C. in China [9]. However, the interaction between water and paper fibres is complex and comprises of several different mechanisms [10], indicating the need for additional research to gain comprehensive understanding of water movement in paper.

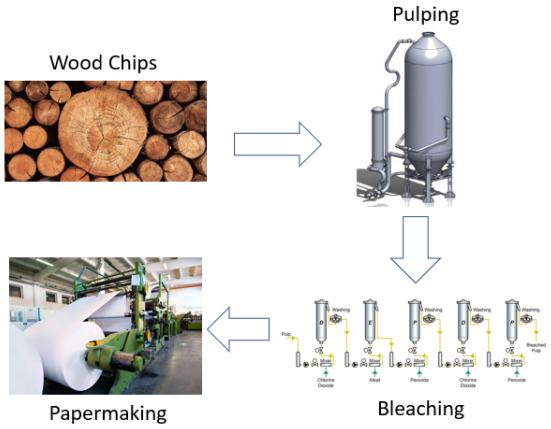

Figure 3.2: Process of papermaking

Cellulose fibres are insoluble in water due to intramolecular and intermolecular hydrogen bonding [11]. Due to this, cellulose chains are arranged in sheets and the hydroxyl groups are pointed outwards from the chains and are oriented in the equatorial plane. Hence there is hydrophobicity above and below these cellulose sheets [5]. However, the orientation of hydroxyl groups cause them to interact with water and make cellulose and in turn paper materials hydrophilic [12]. The interaction of water and the cellulose matrix can be avoided by creating new inner or outer layers that act as a barrier. This can be obtained through so-called sizing i.e, introduction of hydrophobic sites in the bulk of the paper material. Sizing in papermaking is a process of adding hydrophobic agents to the cellulose fibers to reduce the paper's tendency to absorb liquid water, making it more suitable for writing, printing, and preventing moisture [13]. Sizing agents, such as alkyl ketene dimer (AKD), are mixed along with the fibre slurry so as to introduce hydrophobicity throughout the paper [14].

Another method to improve hydrophobicity of paper materials is by coating a poly-

mer layer on the surface of the material. This is commonly done via extrusion or rolling of hot melt polymers. Polymers used for this purpose are typically polyvinylidene chloride (PVdC), polyethylene (PE) and ethylene vinyl acetate (EVA) [15].

The overall durability and strength of the paper depends on a variety of factors such as, i) the strength of individual fibres in the pulp, ii) the average length of the fibres, iii) ability of fibres to bond between each other and iv) the method of paper production and formation of the fiber matrix [16]. As paper found use as a packaging material, sizing, or coating it with polymer-like substances became a requirement, as this would increase its hydrophobicity and reduce the absorbance of water.

When the cellulose pulp is processed in a paper machine and rolled into sheets, the fibres are oriented in a direction called the machine direction (MD), which is the direction along the length of the paper. The direction along the width of the paper is called cross direction (CD) and the through-thickness direction is indicated by ZD. These are shown in the figure 3.3.

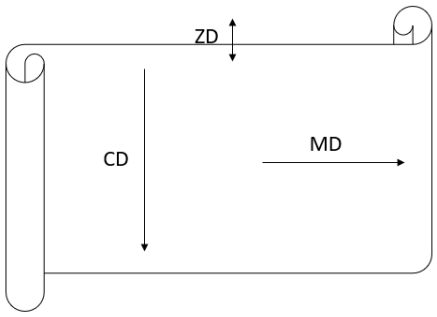

Figure 3.3: Orientation of fibres after paper sheets are rolled

3.1.1 Advantages and Limitations

In combination with other polymers, paper materials have been a popular choice for packaging for several years now. As mentioned previously, the paper is either coated or treated with materials like plastic, aluminium foil or wax to combine both their properties. Paper can provide several properties depending on the materials it is treated with. Some of these properties are given below [15].

- Highly recyclable
- Blocks light due to being opaque
- Easily printable
- Rigid structure and flatness

Despite having these advantages over fossil-based polymer packaging, paper packaging also has some limitations. One of the main drawbacks is the poor barrier

properties, especially against water and water vapour [17]. This is due to the structure of cellulose [18], which is the main component of these fibres, as mentioned earlier.

Paper packaging has been in use for medical devices such as surgical gloves, dressings, catheters and other operation kits. To be suitable for these applications, the paper has to have some special properties such as ability to be sterilized by radiation, seal-able by heat or cold, absence of loose fibers when peeled, and impermeability to microbial entry. For this reason, the papers are coated or laminated with low-density polyethylene (LDPE) or polypropylene (PP), in a specific grid pattern which enables sterilization and heat-sealability. Further, techniques such as high pressure steaming, gas sterilization and radiation using gamma rays are used for sterilization [19]. The maximum pore size of these papers also have to be limited so as to prevent microbial entry [15]. Therefore, there are several factors that determine the usability of papers for application as packaging for medical devices.

3.1.2 Catheter Packaging

This thesis study aims to create fundamental understanding about the properties required for a good paper-based packaging material for single-use catheters. The medical device contains the catheter tube along with a small sachet of salt and water solution used for activation of the hydrophilic catheter surface. Activation refers to the process by which the catheter surface swells up as the polymer coating comes into contact with the salt solution. A hydrophilic surface is crucial as it makes the catheterization more comfortable as well as prevents trauma on the urethra and hence reduces the possibility for additional complications such as urinary tract infection or urethral stricture [20].

The activation is achieved by squeezing the sachet inside the packaging, to let the salt solution spread across the catheter surface. This salt solution is of significance as this is used to activate the catheter surface which then becomes isotonic, i.e, with the same osmotic pressure, to urine and hence ensures smooth and comfortable usage of the catheter [21]. For the reason stated above, the packaging material has to contain this solution in without absorbing it. Even though paper materials can be functionalized through internal sizing or external coating, to prevent water absorption and hence avoid swelling, the functionalization is often not perfect and the fibres can still absorb water to a certain extent. Hence it is crucial to gain deeper understanding about the water absorption mechanisms in these materials, to be able to develop more efficient sizing or coating processes for paper-based packaging depending on the application.

3.2 Mechanisms for Water Transport

Water transport in cellulose fiber-based materials like paper occur through different mechanisms such as diffusion through space between fibres, Knudsen diffusion through pores in fibres, surface diffusion over fibre network and capillary transport through the length of fibres [22].

Diffusion of water between fibres is assumed to follow Fick's law which states that mass flux is directly proportional to the concentration gradients and this movement is assumed to be in the through-thickness direction of the fibre material. Knudsen diffusion is a phenomenon which occurs when the pore size is less than the mean free path of the molecules, and hence collisions with the pore wall is what drives the diffusion process [23]. Capillary transport of water occurs when the water binds to the pore walls like an adhesive. A combination of these adhesive forces and surface tension causes water to move forward [10].

Hashemi et al. [24], found that the moisture intake by paper heavily depends on the amount of moisture already present in the fibres. This increases exponentially with increase in water content in paper. They also found that moisture diffusivity is higher in-plane than through-thickness.

Gupta et al. [22] studied the moisture transport in the through-thickness direction and came up with a model describing the parallel diffusion of moisture through the pores as well as the transport of bound water along the fibres. They found that this model agreed with experimental results on moisture transport through paper, when they got comparable values for diffusivity from the model and the experimental data.

Another interesting phenomena that occurs when paper materials are exposed to moisture or water, is buckling, or bending of the fibres. An example of this is shown in figure 3.4. Lee et al. [25], studied the expansion or swelling of fibres when exposed to water by filming the paper samples across time. Swelling across thickness was found to be quicker than in-plane swelling. For this they measured the time taken for water to reach the other face of the paper and the sides of the paper, respectively. They also computed the strain in the paper when it is aligned in the machine direction and cross direction and strain was found to be higher when aligned in the cross direction.

When paper materials are used as packaging for catheters, water transport can occur in two different ways. Firstly, the packaging may experience leakage of the liquid used to activate the catheter during usage. Secondly, the product will be used in different climates and weather conditions, which may cause moisture from the environment to pass through the packaging. Therefore a thorough understanding of

water transport in paper materials is required to avoid these undesirable situations.

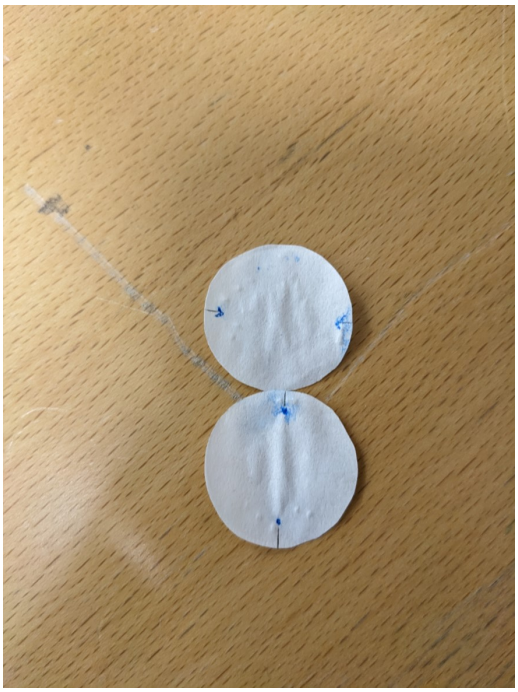

Figure 3.4: Buckling or bending of wet paper.

4

Study of Water Transport in Paper using MRI

NMR or MRI experimental methods have been implemented to investigate the water transport in cellulose-based materials such as thin papers, in various contexts such as water uptake, drying and diffusion of water. To study water transport in such materials, it is important that the fibre network structure is not destroyed as that would alter how the water travels. Being non-invasive and non-destructive, MRI has a great advantage and potential to be used for studying cellulose fibre-based materials.

4.1 Drying of Paper

One of the earliest works which demonstrated this potential of MRI/NMR techniques was Nilsson et al. [1]. They found that earlier methods such as using a composite sample to investigate the drying, did not represent the actual structure of a paper sample. These methods were also destructive and hence the fiber network of the paper was destroyed. They showed that MRI imaging being non-destructive helps to maintain this structure and was able to measure the water distribution with a spatial resolution of 0.39 mm. Achieving a higher spatial resolution without increasing the scan time greatly and decreasing the SNR, was found difficult.

In a study by Harding et al. [26], one dimensional profiles of a drying process of cardboard with a spatial resolution of 15 μm per pixel was acquired. This was combined with a pulsed gradient spin echo (PGSE) method for further insight into the distribution of water through the fiber network. The total thickness of the samples in their study was around 680 μm. The above studies showed how MRI can be very useful to detect as well as obtain quantitative information on water transport in cardboard and paper samples.

4.2 Through-plane Diffusion of Moisture

Leisen et al. [27], used MRI to measure the through-plane moisture distribution in paper samples. Moisture concentrations of 0% to 20% were investigated on sheets of paper pressed together. They were able to visualize how water travels through the paper surface by looking at the images from the MRI, where the brightness of the image signified the quantity of water uptake by the paper. Using this they found that the kinetics of moisture absorption through the cellulose fibres mainly determined the overall rate of water transport through the paper. One limitation they came across is that moisture content below 6% could not be detected by the MRI, as the signal intensities were found to be zero. Transport through spaces between fibres was found to be significant during longer experiment times.

Perrin et al. [28], analyzed the through-thickness liquid distribution in porous media using MRI. They were able to demonstrate a method which gave a spatial resolution of 10 μm and a temporal resolution of 1.3 seconds. With this method they observed the drying of water-based ink on four different papers of thickness ranging from 89 to 129 μm. They could differentiate the papers on the basis of liquid distribution in the z-direction, how far the liquid penetrates into the papers and the kinetics of the drying process. It was concluded that the MRI method is a useful tool to quantify absorption, drying and distribution of water in thin samples such as paper.

Ma et al. [ref], studied the bound-water transport in cellulose-fibre piles using MRI sequences. They used a single-point imaging sequence to record the intensities of bound water across the cross-section of the samples. They use this data to correlate with models which assume sorption equilibrium at any point in the sample. They show that such models can hence be used for good predictions about the properties of drying or absorption of textile materials based on cellulose.

These studies show that MRI sequences can give accurate and valuable insight into the mechanisms and characteristics of water transport in thin materials such as paper and cellulose fibres. The data acquired from such experiments also gave good spatial and temporal resolutions required for these samples. All of these studies also prove the importance of this technique being non-invasive which does not destroy the structure of the samples.

5

Materials and Methods

In this chapter, the methodology used to conduct this study, including a description of the steps, equipment, and techniques used for the analysis of the data is introduced to help readers understand how the study was carried out.

5.1 Materials

In order to accurately characterize the paper samples, it is important to have their specifications. Some of these papers are coated with polymer layers on one side. This is done to improve hydrophobicity of these papers. Table 3.2 presented below outlines the paper samples specifications.

Table 5.1: Paper specifications

Sample name	Coating status	Grammage (gsm)	Caliper (um)
WC gas paper 63 LC	Coated	63	73
AC grid paper KG 9411	Coated	71	70
WC grid paper 70	Coated	70	70
AM SUP NL 60 g	Not-coated	60	70
AM CRSTL 35	Not-coated	35	30.5

5.2 Contact Angle

The wettability of a solid surface by a liquid is characterized by the degree to which the liquid spreads over the surface, and this can be quantified by measuring the contact angle between the liquid and the solid [29]. For cellulose-based materials, the contact angle between a water droplet and a paper sample provides valuable insight into the hydrophilicity or hydrophobicity of the material [30]. One widely used method for determining the contact angle is the sessile drop method, which is favored for its simplicity, low test liquid volume, and minimal sample size needed [29].

5.2.1 Apparatus

The Krüss DSA 100 (Drop Shape Analyzer) is the utilized device for the experimental setup. This instrument features a light source, a high-resolution camera, and a quality zoom lens, enabling an accurate visualization of the liquid drop. The device incorporates three manual axes, facilitating quick and precise positioning of the sample without the need for physical contact, and a syringe to deliver the liquid onto the sample. Krüss DSA 100 can be seen in figure 5.1 below.

Source: https://www.kruss-scientific.com/en/products-services/products/dsa100s

Figure 5.1: Contact angle device Krüss DSA 100.

5.2.2 Method

In the sessile drop method, a small volume of water is deposited onto the surface of the sample using a syringe to ensure consistency in the amount of liquid used for each measurement. The drop is then imaged, and the contact angle formed at the three-phase interface (solid-liquid-gas) is determined using Krüss Advance software that analyse the image.
For accuracy and reliability, the measurements were repeated five times for both sides of each sample. The average value of these measurements, for each side, is then reported. Then, to assess the effect of solution composition on the contact angle, the experiment was performed twice, once using distilled water and once using

a saltwater solution.

5.3 Cobb60 test

The Cobb value, is the mass of water absorbed in a specified time by 1 m^2 of paper sample under 1 cm of water [31].The Cobb60 test is a standard method used to determine the water absorptiveness of a paper sample within a specified time frame of 60 seconds.

5.3.1 Apparatus

1- Paper samples.
2- Scissor.
3- Electronic balance.
4- Stopwatch.
5- Blotting paper.
6- 100 ml measuring cylinder.
7- 100 cm^2 Sample holder with a ring.
8- 10 kg metal roller.

The sample holder with the ring, and the metal roller can be seen in figure 5.2 below.

Source: https://www.unitload.vt.edu/facilities/corrugated-packaging-lab/water-absorption-testing.html

Figure 5.2: Sample holder with a ring, and a metal roller.

5.3.2 Method

The sample is cut to a size slightly larger than the outside dimension of the ring of the holder, and its weight is recorded to the nearest 0.01 g. The sample is then placed on top of a plate, and a ring is placed on top of the sample to prevent any leakage between the ring and the sample. Next, 100 ml of water is rapidly poured into the ring, creating a head of 1 cm, and the stopwatch is started immediately. After 45 seconds, the water is poured out, and after 60 seconds, a sheet of blotting paper is placed on top of the paper sample. A hand roller is then used to move once back and forth over the blotting paper without exerting any extra pressure to remove any surplus water remaining on top of the paper. The paper sample is then reweighed to the nearest 0.01 g, and the weight of the sample paper before the test is subtracted from its weight after the test. The resulting weight in grams is then multiplied by 100 to obtain the weight of water absorbed in g/m^2. The test is repeated three times for each sample, and the average value is reported.

5.4 FTIR

FTIR spectroscopy operates based on the measurement of infrared radiation's absorption or transmission by a sample. It is a valuable analytical technique that enables the identification and quantification of molecular groups present in a sample [32]. Infrared radiation consists of different wavelengths. When infrared radiation interacts with a sample, certain chemical bonds within the molecules will absorb specific wavelengths of the radiation, resulting in peak formations. The collective set of these peaks forms a spectrum, which can then be compared to reference spectra for analysis and identification purposes. The positions of peaks in the spectrum aid in identifying the components, while the intensity of peaks provides insights into their concentration [32]. Infrared spectroscopy has advantages in terms of simplicity and speed, making it easy and fast to measure spectra. Moreover, it offers high sensitivity, allowing routine detection of quantities as low as 10^{-6} grams [32].

5.4.1 Apparatus

The PerkinElmer Spectrum 100 instrument, equipped with the UATR (Universal Attenuated Total Reflectance) accessory using a KRS-5 crystal, is employed for the measurements.
The following figure 5.3 shows where samples placed to run the FTIR.

5.4.2 Method

The sample is carefully positioned on the KRS-5 crystal, and pressure is applied to establish optimal contact between the sample and the diamond crystal to eliminate any potential air gaps that could introduce measurement errors. A background

Source: https://resources.perkinelmer.com/corporate/cmsresources/images/44-74844tch_ftiratr.pdf

Figure 5.3: crystal's surface where samples placed

signal is recorded to establish a reference. After that, the FTIR (Fourier Transform Infrared) measurement is conducted using a specific resolution and a number of scans. The number of scans is important to enhance the signal-to-noise ratio while the resolution is important to identify closely spaced peaks. The number of scans used was 16 and the resolution used was 4 cm^{-1}. The resulting signal is then reported using the Spectrum 10 ES software. In addition, KnowItAll software, developed by Wiley science solutions is utilized to analyze the obtained spectra by comparing and overlaying them with a large database of reference spectra.

5.5 MRI

5.5.1 Apparatus

1- Bruker Avance-III HD NMR spectrometer. It is the MRI instrument used. It has a MiniSWB90 single-tuned 1H quadrature probe with a 40mm diameter and a 7T magnetic field. The MRI device used can be seen in figure 5.4.
2- Paper samples.
3- Scissor.
4- Sample holder stick.
5- Rubber with square opening.
6- Plastic square.
7- Screwable lid.
8- Pipette.

5.5.2 Method

The paper sample was attached to a plastic holder stick. A rubber piece with a square opening at its center was positioned on top of the paper. This rubber

Figure 5.4: Bruker Avance-III HD NMR spectrometer.

component serves the purpose of applying pressure to the paper sample without causing damage to its structure, thereby confining the water within the desired square area. A plastic square was then inserted into the opening of the rubber, acting as a guide to direct the water precisely to the designated area. After that, a lid was securely screwed on top, exerting pressure on the assembly. The lid features a small opening through which a pipette can be inserted to accurately drop water into the square area. A constant amount of water, around 1 mL or approximately 4 drops, is used to ensure complete coverage of the square area. Finally, this prepared setup was carefully inserted into the probe of the MRI device. The explained setup can be seen in figure 5.5. This method was developed in an earlier thesis titled 'Experimental Method Development for MRI Moisture Measurements in Paper Materials' [33].

To ensure consistent alignment while inserting the setup into the MRI probe, a board with an eye hole is utilized. This board provides a fixed viewing angle, allowing the user to maintain a consistent viewpoint while inserting the setup. By utilizing the eye hole, it becomes easier to achieve the same alignment configuration each time, enhancing the reproducibility of the experimental setup.

Once the water is dropped into the setup using the pipette, it is immediately inserted into the MRI probe. The 1-D multiple-slice multiple-echo (MSME) sequence is then initiated and run for a duration of 30 minutes. Following this, a 2-D MSME sequence lasting 32 seconds is performed to confirm the alignment of the setup. This sequence of steps is carried out for both sides of all five paper samples.

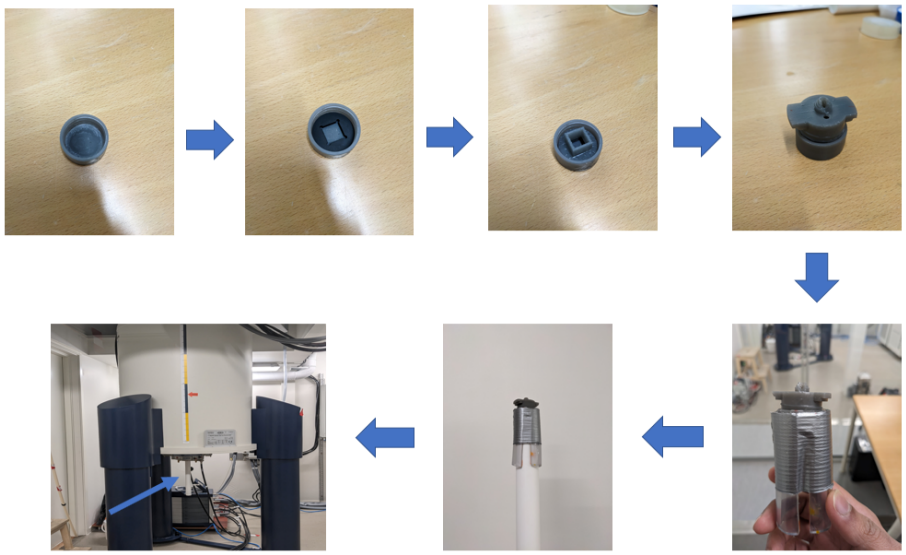

Figure 5.5: The setup used for sample insertion into MRI probe.

5.5.3 MRI Scan Settings

There are several parameters in the MRI which affect the scan time and the Signal-to-Noise Ratio (SNR) of the output as discussed in section 2.2. More number of repetitions give better temporal resolution. However, it greatly increases scan time as the other parameters have to be changed to get a good SNR. In our method, the scan time was fixed first as 30 minutes, to be able to compare all the samples. Since this was fixed the other parameters were optimized around it to get a good SNR. This was achieved by decreasing the number of repetitions to 114, which still gives a temporal resolution of 15.78 seconds, and increasing the Number of Signal Averages (NSA) to 8 to improve the SNR. These parameters are given below both for the 1-D MSME sequence and the 2-D MSME sequence in tables 5.2 and 5.3 respectively.

Table 5.2: MRI settings for 1-D MSME sequence.

Parameter	**Value**
Number of Repetitions	114
Number of Signal Averages	8
Scan Time	30 minutes
Slice Thickness	3.9 mm
Field of View	5 mm
Echo Time	7.58 ms
Repetition Time	2000 ms
Slice Direction	Sagittal

Table 5.3: MRI settings for 2-D MSME sequence.

Parameter	**Value**
Number of Repetitions	1
Number of Signal Averages	1
Scan Time	32 s
Field of View	40 mm, 40 mm
Echo Time	5.02 ms
Repetition Time	500 ms

6

Results and Discussion

6.1 Contact Angle

Contact angle measurements are valuable for assessing the wettability properties of paper samples and determining their hydrophobic or hydrophilic nature. A contact angle above 90 degrees signifies a hydrophobic (water-repelling) surface, whereas a contact angle below 90 degrees suggests a hydrophilic (water-attracting) surface [34]. To provide a visual representation of the contact angle measurements interpretation, please refer to Figure 6.1 which was adapted from [35]. The accompanying Table 6.1 presents contact angle values obtained for the five paper samples (treated side) at the middle (CA(M)), left (CA(L)), and right (CA(R)) sides in degrees [°]. The rest of the values are given in appendix B.

Table 6.1: Contact angle values of the paper samples (treated side)

Sample name	CA(L)	CA(M)	CA(R)
WC gas paper 63 LC	117.25°	117.71°	118.17°
AC grid paper KG 9411	91.51°	91.40°	91.30°
WC grid paper 70	85.94°	85.82°	85.70°
AM SUP NL 60 g	37.57°	33.90°	30.23°
AM CRSTL 35	29.61°	30.43°	31.25°

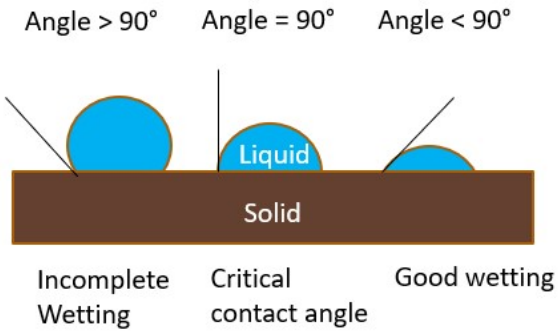

Figure 6.1: Visual representation of the contact angle measurements interpretation.

6.2 FTIR

At the beginning, FTIR results were employed to differentiate between the treated and non treated sides of the paper sample by comparing the obtained spectrum to a reference. The analysis showed that the untreated side of the paper samples exhibits a spectrum similar to that of cellulose, the primary component of paper. Figure 6.2 shows the spectrum of the untreated paper (AM SUP NL 90 g) alongside the spectrum of cellulose, both presented in the same graph. All graphs presented in this section are created using the KnowItAll software by Wiley science solutions. The X-axis represents wave length in cm^{-1}, the Y-axis represents absorbance. Notably, the two spectra exhibit a remarkable match, indicating a high degree of similarity between this sample and cellulose. The non-treated side in all paper samples has a similar spectra. The spectra for all the samples can be found in appendix A.

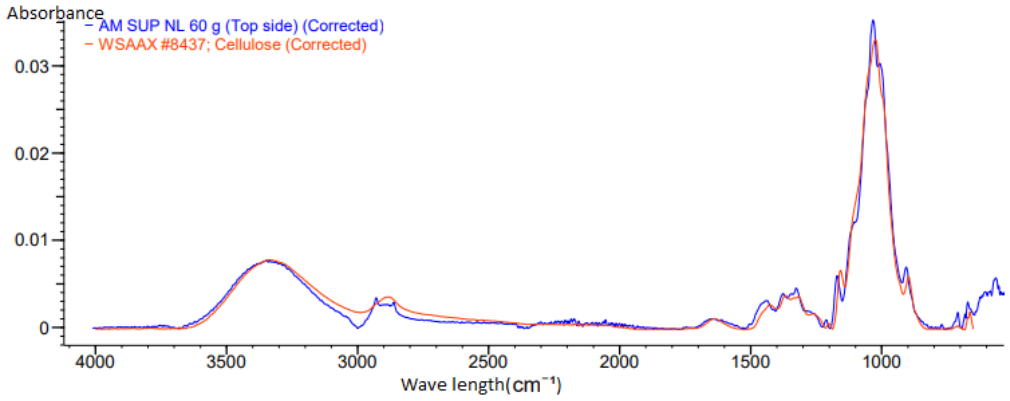

Figure 6.2: Cellulose spectrum overlaid with AM SUP NL 90 g paper spectrum

Moreover, FTIR was then used to identify the type of treatment applied to the paper samples. By examining the spectrum, characteristic peaks corresponding to specific functional groups or chemical species can be observed, providing valuable insights into the nature of the treatment.

Through a comprehensive analysis of the spectra and comparing them to reference spectra of common materials used for paper treatment, the specific materials applied to treat the paper samples were identified to a large extent. The results revealed that AC grid paper KG 9411 and WC grid paper 70 share the same treatment material, although the extent of treatment differs between the two samples since they have identical spectra differs only in signal intensity. Both spectra can be seen in figure 6.3. On the other hand, WC gas paper 63 LC was found to be treated with a different material compared to the aforementioned samples.

Both grid papers, AC grid paper KG 9411 and WC grid paper 70, were observed to be treated with a combination of polyethylene and polystyrene. Figure 6.4 illustrates the spectra of AC grid paper KG 9411 overlaid with the spectra of ARCEL, which

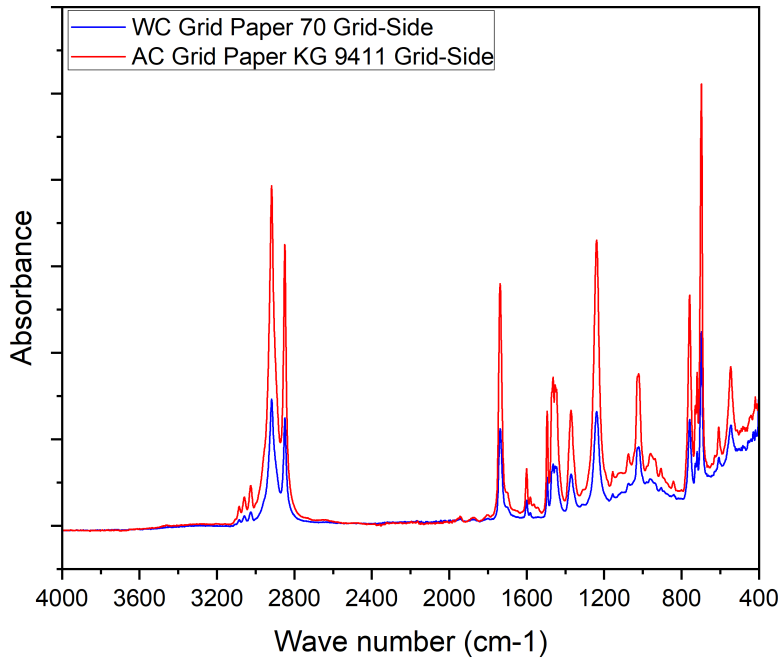

Figure 6.3: Spectra of AC grid paper KG 9411 and WC grid paper 70.

is known to be a mixture of polyethylene and polystyrene. The peaks in the spectra align with each other, indicating similarities in the chemical components. However, it should be noted that the intensity of the peaks is not the same due to the different percentages of each component present in the samples.

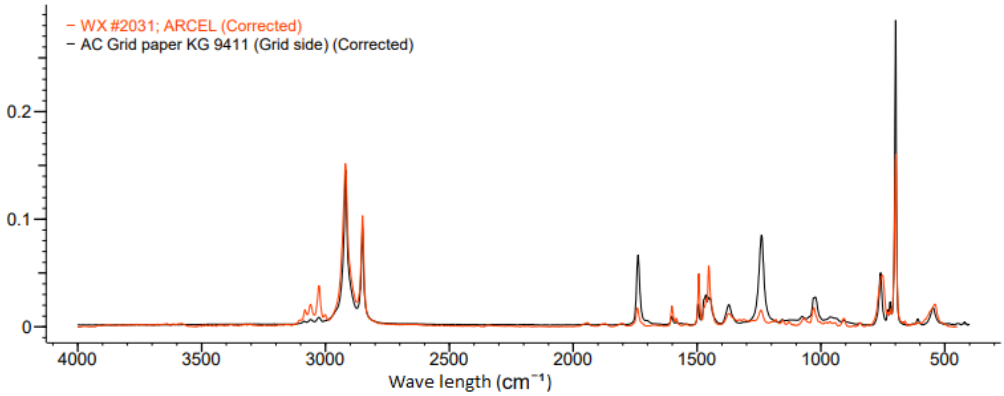

Figure 6.4: AC grid paper KG 9411 spectrum overlaid with ARCEL spectrum

The mechanical properties of paper, including rigidity, flexibility, and tensile strength, as well as its water absorbency, can be influenced by the type of treatment applied [36]. In this study, the focus was primarily on investigating the water absorbency of the samples.

Polystyrene has low surface energy and poor polarizability which make it hydrophobic [37]. Also, it can be seen that polyethylene is hydrophobic when looking at the non-polar molecular structure of it which constitute of only hydrogen atoms that are connected to a carbon backbone [38].
Based on the hydrophobic nature of both materials, it can be hypothesized that a blend of the two would also result in a hydrophobic mixture, that can be used to enhance the hydrophobicity of the paper samples, which can be confirmed with the obtained contact angles showed in table 6.1. Another observation, is that the extent of the coating directly impact the water repellency of the paper surface this can be seen when comparing the contact angle of AC grid paper KG 9411 to the contact angle obtained for WC grid paper 70,in table 6.1, where both are treated with the same coating material but with different coating thickness.
On the other hand, WC gas paper 63 LC is treated with ethylene/vinyl acetate co-polymer. Figure 6.5 displays the spectra of WC gas paper 63 LC overlaid with the spectra of ethylene/vinyl acetate co-polymer 86/14. The majority of peaks in the spectra align with each other, indicating the presence of the main material used to treat the paper. However, there are two small peaks in the range of 1500-1600 cm^{-1} that do not align perfectly, suggesting the possible presence of another component in a small amount. Nonetheless, the main material responsible for treating the paper has been identified as ethylene/vinyl acetate co-polymer.

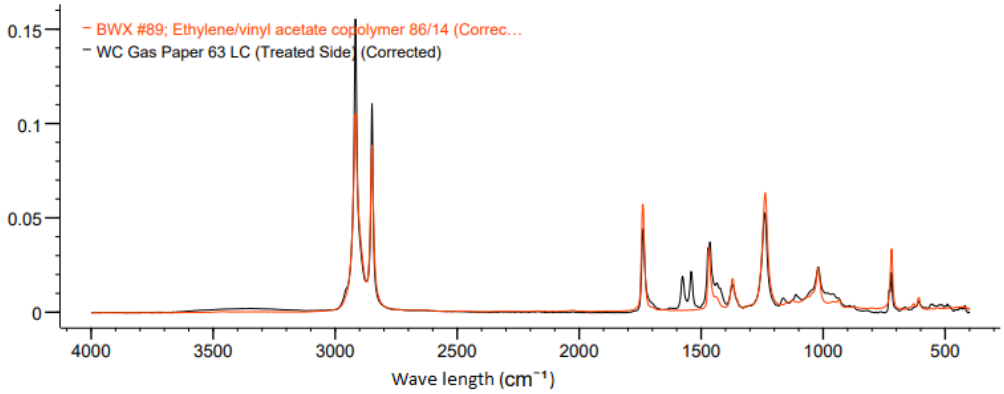

Figure 6.5: WC gas paper 63 LC spectrum overlaid with the spectrum of ethylene/vinyl acetate co-polymer

The treatment of the paper samples with ethylene/vinyl acetate co-polymer is to enhance samples hydrophobicity. This is because of the presence of ethylene in the ethylene/vinyl acetate co-polymer, as it is responsible of the hydrophobic properties of the coating [39]. On the other hand, vinyl acetate serves the purpose of improving flexibility and adhesion to the substrate [40]. In support of this, Table 6.1 provides an evidence, as the paper sample that is coated with ethylene/vinyl acetate co-polymer exhibits a high contact angle which indicate an increased resistance to wetting and confirm the enhanced hydrophobicity achieved through the treatment.

6.3 MRI Results

6.3.1 Interpretation

As mentioned in the methods section, there are two sequences run using the MRI. The 1-D MSME sequence gives quantitative data regarding the signal intensity of water over time across the thickness of the setup, while the 2-D MSME sequence also gives an image which depicts the water contrasted against the rest of the setup. This shows the visual representation of the water as seen from the top and sides. Figure 6.6 shows the image obtained from the 2-D sequence.

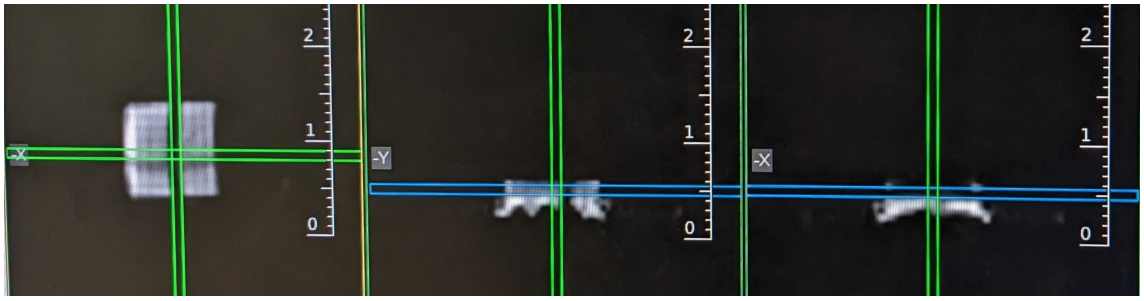

Figure 6.6: 2-D MSME images obtained from the MRI. The top view is shown in the first image from the left and the side views in the following images.

The 1-D MSME sequence produces data of signal intensities of water over time and at each point in space. Figure 6.7 shows an example of this graph which is obtained after processing the raw data from the MRI in MATLAB.

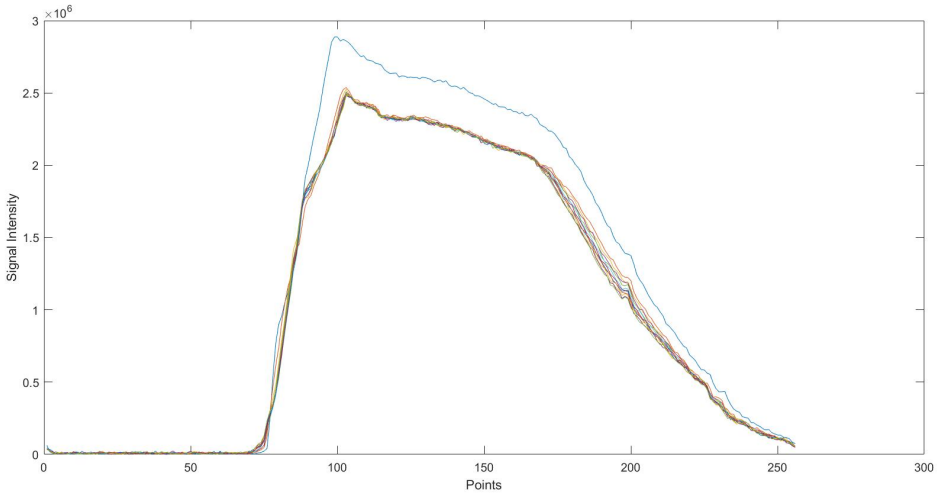

Figure 6.7: Graph representing signal intensity vs number of points obtained from the 1-D MSME sequence.

In figure 6.7, the y-axis represents the signal intensity of water and the x-axis represents the number of points across a specified length along the thickness of the setup.

This length is shown in figures 6.8 and 6.9. This length is divided into 256 points. The slice thickness for the MRI scan was set to 3.9 mm, which means each point represents $\frac{3.9}{256}$ μm or 15.23 μm in real length.

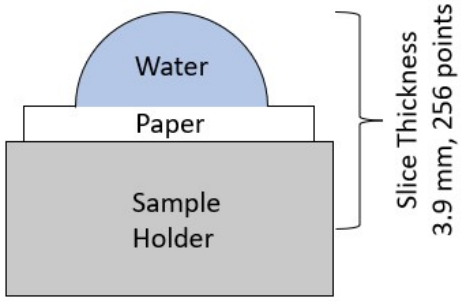

Figure 6.8: Simplified setup

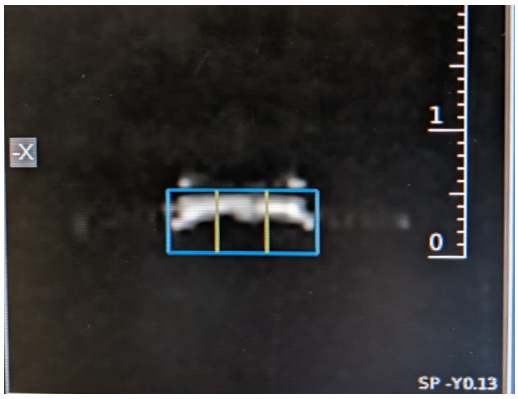

Figure 6.9: Slice side view

The next step in the interpretation of these results is classifying the signal from MRI into mainly three regions. These are the bulk water, paper, and the region below the paper. In figure 6.10, the curve on top, shown as blue, represents the initial repetition of the experimental trial, followed by an additional 113 repetitions. Considering that a total of 114 repetitions were conducted within a 30-minute time frame, the duration for each individual experiment was determined to be $\frac{30}{114}$ minutes or 15.79 seconds. The figure shows every 10 repetitions. It can be observed from the figure that the signal intensity at the right end of the length scale is decreasing with each repetition which indicates it is decreasing with time. This indicates that the signal from the bulk water is decreasing which might be linked to the water intake by the paper. Further, the direction of the arrow indicates the decrease in the intensity over each repetition, i.e., over time.

Figure 6.11 shows a zoomed-in version of the Figure 6.10. Here it can be observed that the blue curve is down and the signal intensity here increases with time. This, along with the fact that the overall intensities are much lower than that in the bulk water, point to the conclusion that this is the range of points where the thickness of the paper is located. Further, the region of points where the signal intensities over time are zero, indicate the points below the paper and in the sample holder, where there is no water at any time. Here, the direction of the arrow represents the increase in signal intensity over each repetition, i.e., over time.

This interpretation was further used to extract how the signal intensity changes over time at each point in the region of paper. This data would help in comparing the papers as one would get more insight into the water intake rates of the papers along with the time it takes for each of them to saturate with water.

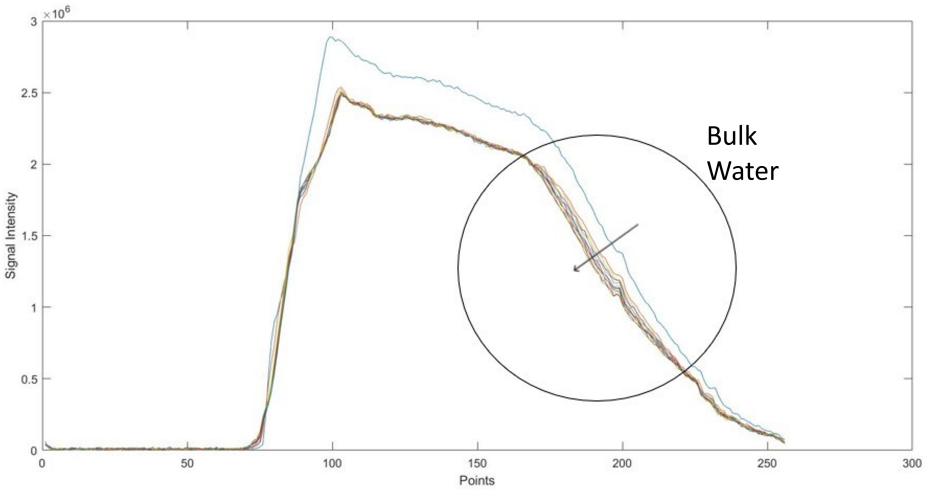

Figure 6.10: The circled area in the above graph depicts the area where there is a decrease in signal intensity of bulk water.

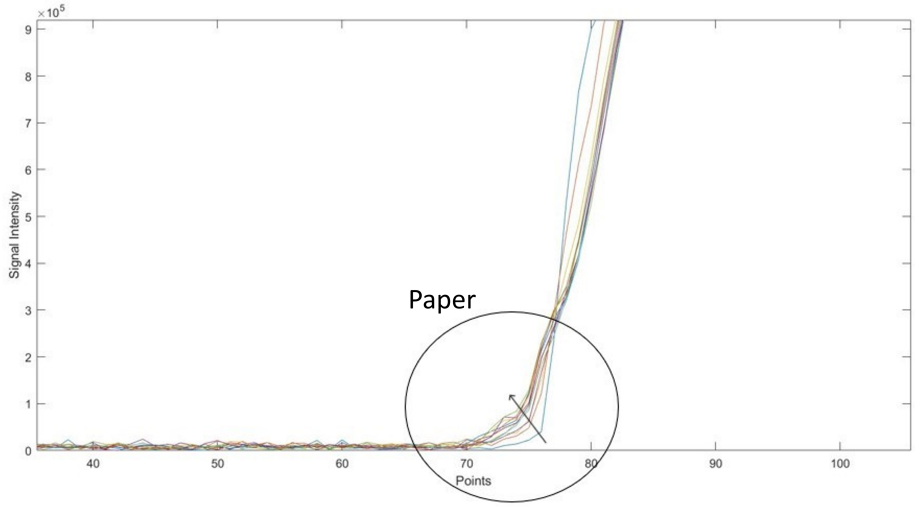

Figure 6.11: The circled area in the above graph depicts the area where there is an increase in signal intensity. This is most likely the region of points inside the paper.

6.3.2 Initial results

For the first set of experiments, the two sequences were run on all five samples of paper, giving results which could be interpreted as described earlier. The graphs for intensity vs the length scale for the AC Grid Paper KG 9411 are shown in figure 6.12. Using these graphs, the data for water transport into the paper could be extracted at each point using the interpretation described earlier.
However for the other paper samples, these graphs showed sudden rises in the signal intensity at several points. Examples of these are shown in figure 6.13. Initially, these rises were interpreted as the increase in water intensity due to swelling of the paper. However, the intensities were much higher than the maximum intensity seen

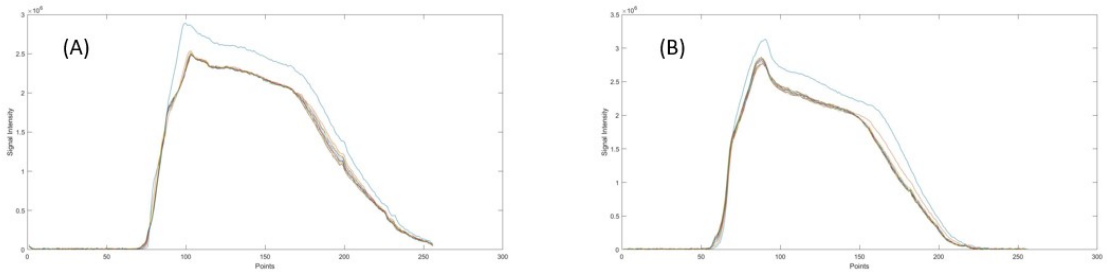

Figure 6.12: Signal intensity vs number of points for AC Grid Paper KG 9411, (A) Grid side and (B) Non-Grid side.

in the results for AC Grid Paper KG 9411. The drastic differences in the signals meant that a useful comparison could not be done and hence it was concluded that an error in the setup could have caused this.

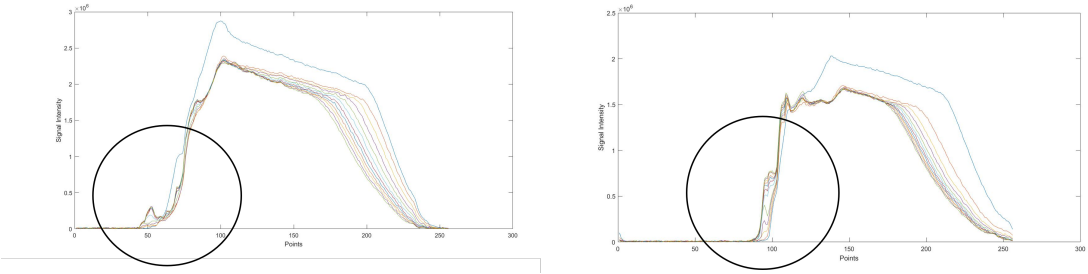

Figure 6.13: Signal intensity vs number of points for WC Gas Paper 63 LC. Circled areas show the sudden increase in the signal intensity.

To confirm this, the same MRI sequences were run on a material which was completely hydrophobic and a sample of Parafilm material was chosen for this. The findings from this test and the following modification in the setup is described in the next section.

6.3.3 Method Improvement

As previously mentioned, certain samples showed a sudden increase in signal intensity during MRI scans. To investigate this, an MRI scan was conducted on a parafilm using the same experimental setup. This was performed to observe the intensity versus points graph knowing that parafilm does not possess water-absorbing properties. Figure 6.14 displays the resulting signal intensity graph obtained from this investigation.
The obtained graph from the MRI scan of the parafilm did not align with the anticipated expectations, revealing unexpected increase in signal intensity at certain points. This outcome challenges the initial assumption that the signal intensity spikes were connected to the buckling of the paper samples. Since parafilm does not

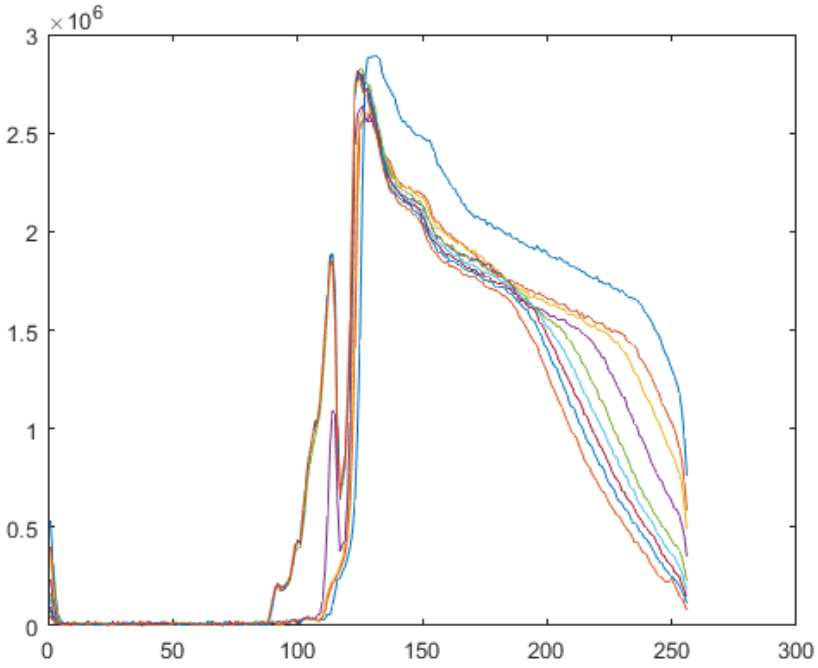

Figure 6.14: Signal intensity vs Number of points for parafilm

absorb water and is not prone to buckling, it eliminates the possibility that the sudden increase in the signal intensity is caused by this factor. To further investigate the underlying cause, a closer look on the images generated from the 2D-MSME scan was done. Figure 6.15 displays the resulting image obtained from the scan performed on the parafilm.
The image on the left in Figure 6.15 clearly shows water going out from the designated square area, and also in the side view, bright spots can be observed at the sides of the bulk water, leading to water accumulation underneath the parafilm and below the rubber component. This observation suggests that the sudden increase in signal intensity may be attributed to the presence of water outside the desired area. Moreover, similar findings were observed in all samples that exhibited sudden signal intensity increases, indicating a direct correlation between these signal anomalies and the presence of water outside the designated square area.

After this, all the samples were re-scanned with the lid tightly screwed while ensuring the alignment remained unchanged, to mitigate the issue of water escaping the desired area.

Figure 6.16 presented below displays the side view image obtained from the 2D-MSME scan of the parafilm after tightening the lid, illustrating the absence of water outside the desired area. This confirms that the measures taken effectively prevented water from escaping the desired region. Additionally, Figure 6.17 portrays the intensity graph obtained from the same sample, demonstrating an anticipated signal intensity without any sudden increases. This result indicate that no water

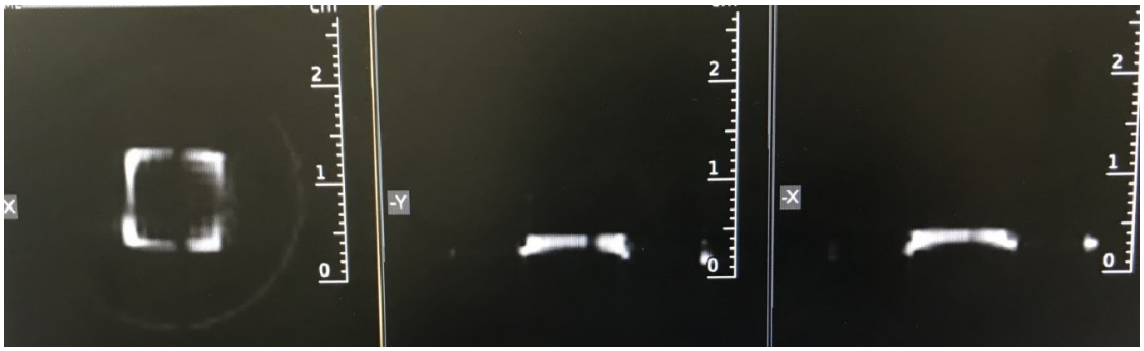

Figure 6.15: 2D-MSME Image of the parafilm.

was absorbed into the parafilm during the scanning process, which goes well with the expected behavior of the material.

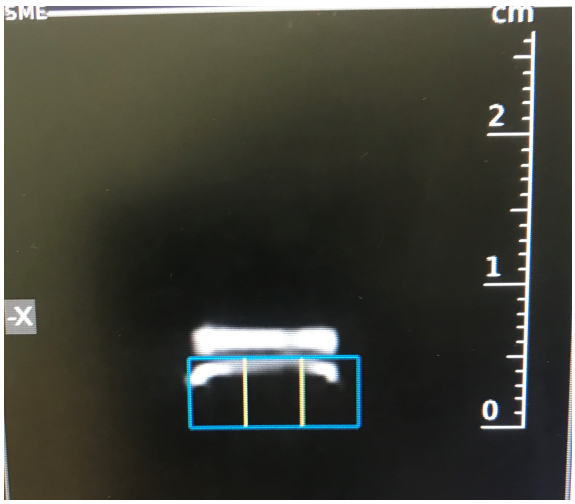

Figure 6.16: 2D-MSME side view image of parafilm after tightening the lid.

Ensuring the alignment of the setup is also important to obtain reliable and comparable results. Any alteration in the alignment can have significant effects on the outcomes. For example, if the square is rotated, it will introduce additional area into the slice. Since the signal intensity is averaged, such alterations can lead to changes in the resulting signal intensity, ultimately impacting the overall accuracy and interpretation of the data. Figure 6.18 and figure 6.19 below shows a well aligned setup and one with rotated square.

6.3.4 Further Results

The improvement in the method gave better results from the MRI sequences and the information extracted could be better compared since the setup was more robust. The sequences were run with pure water as well as 3 w/v% NaCl in distilled water on both sides of all samples.

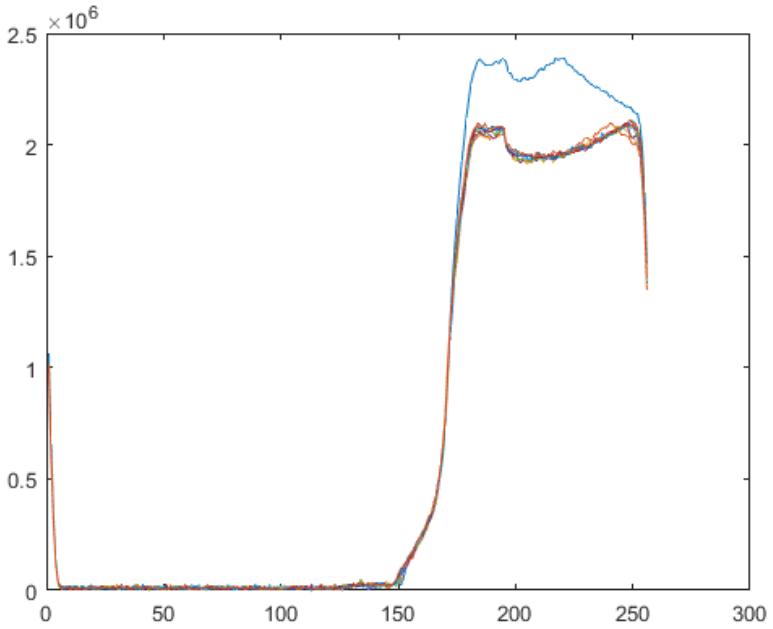

Figure 6.17: Signal intensity vs points for parafilm after tightening the lid.

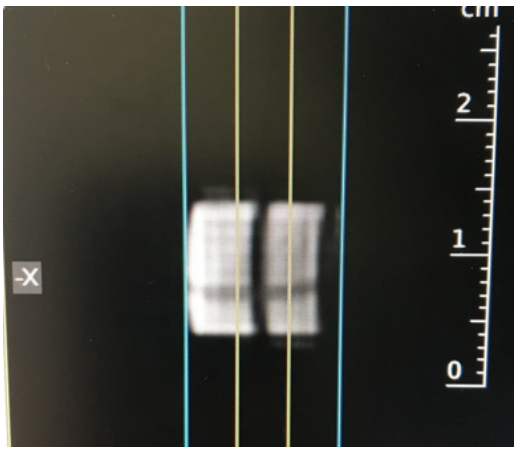

Figure 6.18: Well aligned setup.

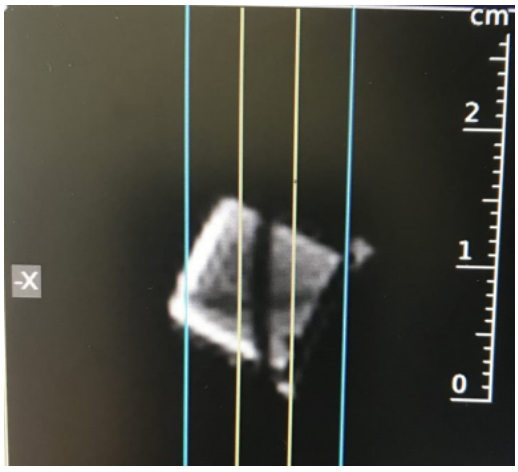

Figure 6.19: Rotated alignment.

The results for water on the treated or coated sides of the samples are given in figure 6.20. Here the y-axis corresponds to the water signal intensity and the x-axis corresponds to time in minutes. Further, the different curves in each graph represent a set of points across the cross-section of the paper.

From this graph, it is possible to differentiate between the papers based on the amount of water absorbed in 30 minutes, as the intensity scale has been normalized. The trend seen here is that the WC Gas Paper 63 LC and the AC Grid Paper KG 9411 absorb the least amount of water, followed by the AM SUP NL 60 g and AM Crstl 35. The WC Grid Paper 70 absorbs the most amount of water. This trend

Table 6.2: Cobb60 Values.

Paper	**Cobb Value in $\frac{g}{m^2}$**
WC Gas Paper 63 LC	8
AC Grid Paper KG 9411	18
AM SUP NL 60 g	41
AM Crstl 35	34
WC Grid Paper 70	44

was also confirmed by the Cobb60 values which are given in table 6.2 for reference. Further, time lapse videos of how water is absorbed over these samples, also confirmed the same trend.

Similar plots were obtained for experiments with water on the non-treated sides of all samples. These are compiled in figure 6.21. Here, except for the WC Grid Paper 70, the others have comparable absorption of water based on the signal intensities. This can be explained by the fact that all these sides are not-treated and hence the structure is also similar, which is further confirmed by the FTIR results. The WC Grid Paper 70 still absorbs much more water compared to the rest as the water travels in-plane as well as through-thickness of the sample.

Further the results for the same MRI sequences on salt water (3w/v%) are presented. Figure 6.22 shows the data for treated sides and figure 6.23 shows the data for non-treated sides. For the treated sides, the trends in the signal intensity are similar to water. For the non-treated sides the WC Gas paper absorbs the least while the rest of them have comparable signal intensity trends. The signal is more noisy here as the total signal is reduced compared to water due to the presence of salt.

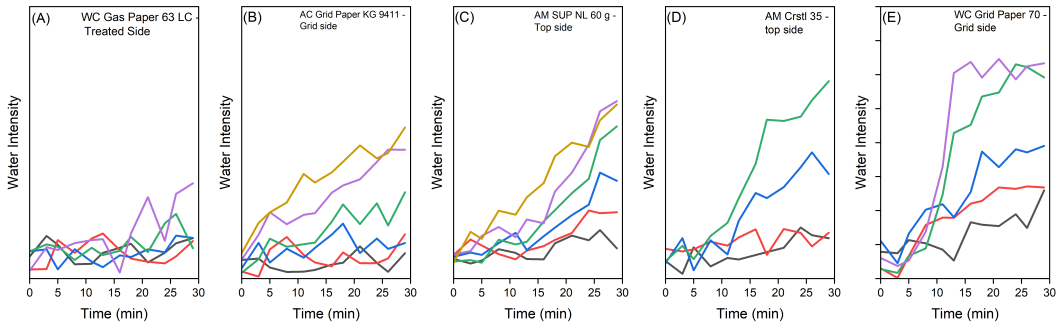

Figure 6.20: Water Signal Intensity vs Time for multiple points across cross-section for the treated sides of all samples

Another interesting value to compare the papers is the time taken to saturate with water. This data can be extracted from the intensity vs time plots shown above,

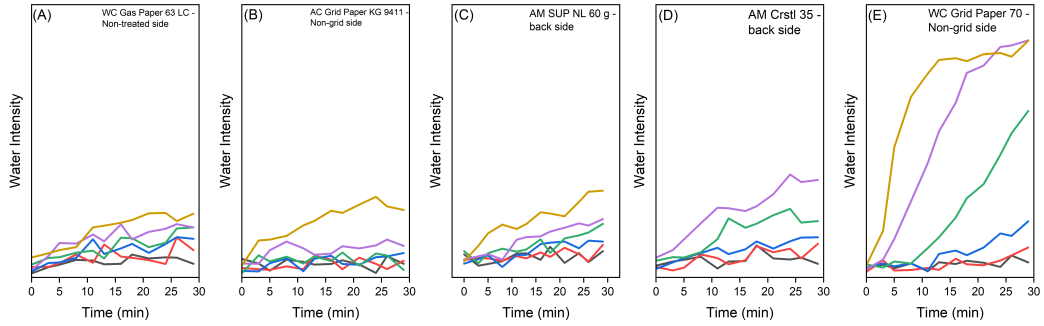

Figure 6.21: Water Signal Intensity vs Time for multiple points across cross-section for the non-treated sides of all samples

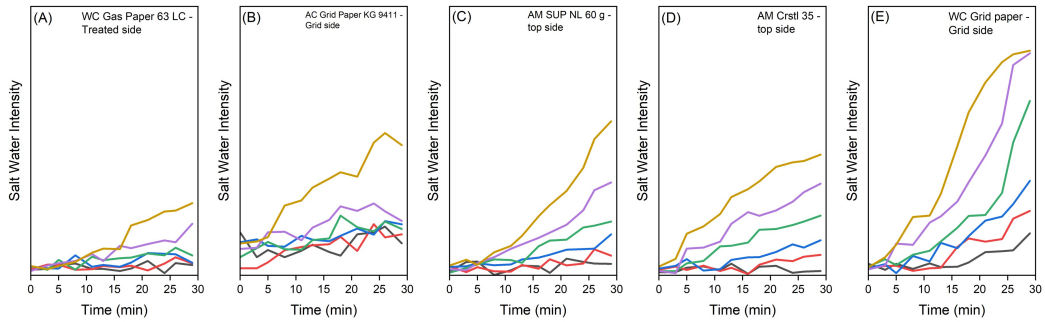

Figure 6.22: Salt Water Signal Intensity vs Time for multiple points across cross-section for the treated sides of all samples

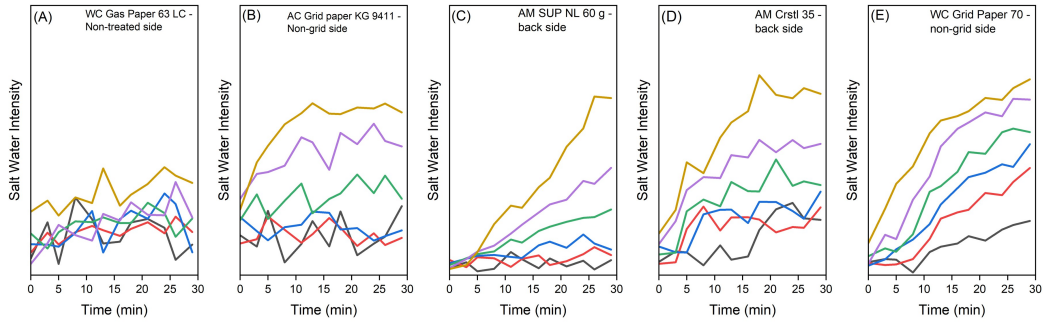

Figure 6.23: Salt Water Signal Intensity vs Time for multiple points across cross-section for the non-treated sides of all samples

by looking at the time where the curves plateau. The values for water are given in table 6.3. From this data, it can be seen that the WC Grid Paper 70 saturates quickly with water, which is also confirmed by the MRI results. Of the treated sides, WC Gas Paper 63 LC has the longest saturation time. However, the AM SUP NL 60 g and the AM Crstl 35 also have similar times. This could be due to the fact that they absorb more water while the WC Gas Paper 63 LC does not absorb much compared to them.

Table 6.3: Saturation times for water.

Paper	Treated Side	Non-treated side
WC Gas Paper 63 LC	24 min	18 min
AC Grid Paper KG 9411	16 min	21 min
AM SUP NL 60 g	24 min	26 min
AM Crstl 35	24 min	26 min
WC Grid Paper 70	13 min	5 min

As seen in Figure 6.20, the WC Grid Paper 70 absorbs more water than the other samples. This trend continues in Figure 6.21, where water is applied to the non-treated side of the samples. Even though water is applied to the non-treated side, some samples still absorb less water. This could possibly be due to the effect of the treatment on the other side acting as an internal barrier. However, when WC Grid Paper 70 is compared to AM SUP NL 60g, which lacks any treatment, WC Grid Paper 70 shows a higher water absorption level. This means that the inherent properties and physical structure of WC Grid Paper 70 might be the primary factors contributing to its higher water intake levels.
Moreover, when comparing the treated and non-treated side of the WC grid paper 70, there's no significant difference, there is only a small delay before the signal intensity starts to increase. This is likely due to the treatment layer. Although the treatment material used is the same as the one used for AC grid paper KG 9411, the sample with the second lowest water intake, and visually the grid structure on the surface of both samples looks similar, but it is showed earlier in FTIR section that the amount of treatment material used is less in WC grid paper 70, which can be confirmed by the fact that AC grid paper KG 9411 sample is heavier by 1 g/m^2 as can be seen in table 5.1. This could mean that the treatment layer on the WC Grid Paper 70 is not thick enough to effectively eliminate water absorption or some tiny cracks or defects in the coating lead to the transportation of water into the paper.

As mentioned earlier in FTIR section, Both WC gas paper 63 LC and AC grid paper KG 9411 are treated with hydrophobic materials, but to interpret why WC Gas Paper 63 LC absorbs less water than AC Grid Paper KG 9411, or why it exhibits a higher contact angle, remains a challenge. Numerous key factors, such as the treatment layer's thickness, the percentage of materials presented in each blend, uniformity of treatment layer, and paper physical structure can influence these outcomes. Our hypothesis is that the ethylene/vinyl acetate co-polymer might have outperformed the polyethylene and polystyrene mixture due to the presence of vinyl acetate, which possibly enhanced the blend's adherence to the sample. An additional factor to consider is the surface texture. The surface of WC Gas Paper 63 LC is smoother compared to AC Grid Paper KG 9411. This difference in surface

smoothness might have influenced the water absorption and contact angle results.

Surprisingly, the AC grid paper KG 9411 exhibited a slightly better performance on the non-grid side compared to the grid side, which contradicted the initial expectations. Both sides showed hydrophobic characteristics, as indicated by contact angles greater than 90°. However, the non-grid side, which corresponds to the non-treated side, exhibited a higher contact angle.
This unexpected observation could be because of the surface texture, the non-grid side is smoother than the grid side, or changes in paper properties resulting from the treatment process. It is also possible that the non-grid side may have residual substances or impurities that could have influenced the contact angle results.
AM SUP NL 60 g and AM CRSTL 35 didn't show any difference between top side and back side in the resulted spectra, so it's hard to know why a specific side perform better than the other, and it is not possible to compare them with the trend in the other samples.

To gain a better understanding of the paper samples and their treatment, additional tests should be done. Micro-graphs can provide valuable insights into the physical structure of the papers and the coatings, allowing for a detailed examination of their morphology, surface features, and any potential variations or defects. Furthermore, chemical analysis can help in determining the composition of the coatings and identifying if any residual substances is presented.

7

Conclusions and Future Work

This study focused on understanding the water transport behaviour of five different paper samples using the Magnetic Resonance Imaging technique. This is to know if these can be used as packaging material for catheter devices which require that the packaging can resist water absorption for at least 5 to 10 minutes.

The MRI scans provided a temporal resolution of 15.78 seconds and a spatial resolution of 15.23 μm. With this the intensity of water and 3w/v% salt water was analysed over a time period of 30 minutes for both sides of all samples. Using this data, it was found that the papers could be differentiated on the basis of their water intake rates or the amount of water absorbed over time. Further, the times taken for each paper sample to saturate with water was also found. This data would give a good insight into the quality of these samples for this specific packaging application.

WC gas paper 63 LC and AC grid paper KG 9411 exhibited the best performance among all tested samples. They showed a contact angle greater than 90°, a Cobb value below 20 g/m^2, and demonstrated lower water take-up, which was evident from the observed lower signal intensity in MRI analysis. These results indicated their superior hydrophobicity and reduced water absorption when compared with the other samples.

The fact that a high spatial resolution was achieved without damaging the fibre network is proof of the compatibility of MRI for such studies, as it is non-invasive and non-destructive. For these samples, it would also be interesting to compute the diffusivities of water using diffusion sequences in the MRI. For future studies however, the sample setup can be optimized by changing the screw system to a system where pressure can be exerted without disturbing the alignment of the sample inside the holder. Nevertheless, this study proves that using the MRI technique is considerably useful in studying the water transport in thin paper samples.

References

[1] L Nilsson, S Mansson, and S Stenstrom. Measuring moisture gradients in cellulose fibre networks: An application of the magnetic resonance imaging method. *Journal of pulp and paper science*, 22(2):J48, 1996.

[2] Brian M Dale, Mark A Brown, and Richard C Semelka. *MRI: basic principles and applications*. John Wiley & Sons, 2015.

[3] Govind B. Chavhan. *MRI Made Easy (for Beginners)*. JP Medical Publishers Ltd, 2nd edition, 2013.

[4] Zhong Liu, Huimei Wang, and Lanfeng Hui. Pulping and papermaking of non-wood fibers. In Salim Newaz Kazi, editor, *Pulp and Paper Processing*, chapter 1. IntechOpen, Rijeka, 2018.

[5] Göran Gellerstedt, Monica Ek, and Gunnar Henriksson. Wood chemistry and wood biotechnology, 2009.

[6] Henrik Vibe Scheller and Peter Ulvskov. Hemicelluloses. *Annual review of plant biology*, 61:263–289, 2010.

[7] Richard P. Wool. 16 - lignin polymers and composites. In Richard P. Wool and Xiuzhi Susan Sun, editors, *Bio-Based Polymers and Composites*, pages 551–598. Academic Press, Burlington, 2005.

[8] Peder J Kleppe. Kraft pulping. *Tappi*, 53(1):35–47, 1970.

[9] J. Needham and T. Tsuen-Hsuin. *Science and Civilisation in China, Part 1, Paper and Printing*. Science and Civilisation in China. Cambridge University Press, 1985.

[10] Pekka Salminen. *Studies of water transport in paper during short contact times*. Åbo Akademi University Turku, Finland, 1988.

[11] Clemens M Altaner, Lynne H Thomas, Anwesha N Fernandes, and Michael C Jarvis. How cellulose stretches: synergism between covalent and hydrogen bonding. *Biomacromolecules*, 15(3):791–798, 2014.

[12] Pieter Samyn. Wetting and hydrophobic modification of cellulose surfaces for paper applications. *Journal of Materials Science*, 48(19):6455–6498, 2013.

[13] Antti Korpela, Aayush Kumar Jaiswal, and Jaakko Asikainen. Effects of hydrophobic sizing on paper dry and wet-strength properties: A comparative study between akd sizing of nbsk handsheets and rosin sizing of ctmp handsheets. *BioResources*, 16(3), 2021.

[14] Monika Stankovská, Juraj Gigac, Michal Letko, Elena Opálená, et al. The effect of surface sizing on paper wettability and on properties of inkjet prints. *Wood Res*, 59(1):67–76, 2014.

[15] Jonathan Fowle and Mark J Kirwan. Paper-based flexible packaging. *Handbook of Paper and Paperboard Packaging Technology, 2nd ed.; Kirwan, MJ, Ed*, pages 91–124.

[16] Tero Taipale, Monika Österberg, Antti Nykänen, Janne Ruokolainen, and Janne Laine. Effect of microfibrillated cellulose and fines on the drainage of kraft pulp suspension and paper strength. *Cellulose*, 17:1005–1020, 2010.

[17] Supattra Klayya, Nattaya Tawichai, Uraiwan Intatha, Han Zhang, Emiliano Bilotti, and Nattakan Soykeabkaew. Sustainable nanocomposite coating for moulded pulp with enhanced barrier properties for food packaging applications. *Polymer International*, 72(3):323–332, 2023.

[18] M. E. Parker, J. E. Bronlund, and A. J. Mawson. Moisture sorption isotherms for paper and paperboard in food chain conditions. *Packaging Technology and Science*, 19(4):193–209, 2006.

[19] Bohdan Czerniawski. Flexible packaging of disposable medical devices—a review. *Packaging Technology and Science*, 3(4):203–217, 1990.

[20] Xi Liao, Yuwei Liu, Shiqi Liang, and Ka Li. Effects of hydrophilic coated catheters on urethral trauma, microtrauma and adverse events with intermittent catheterization in patients with bladder dysfunction: a systematic review and meta-analysis. *International Urology and Nephrology*, 54(7):1461–1470, 2022.

[21] This information was obtained from conversations with Maria Gunnarsson and Åsa Westling from Wellspect Healthcare.

[22] Hemant Gupta and Siddharth G Chatterjee. Parallel diffusion of moisture in paper. part 1: Steady-state conditions. *Industrial & engineering chemistry research*, 42(25):6582–6592, 2003.

[23] Kelley L Spence, Richard A Venditti, Orlando J Rojas, Joel J Pawlak, and Martin A Hubbe. Water vapor barrier properties of coated and filled microfibrillated cellulose composite films. *BioResources*, 6(4), 2011.

[24] SJ Hashemi, VG Comes, RH Crotogino, and WJM Douglas. In-plane diffusivity of moisture in paper. *Drying technology*, 15(2):265–294, 1997.

[25] Minhee Lee, Seungho Kim, Ho-Young Kim, and L Mahadevan. Bending and buckling of wet paper. *Physics of Fluids*, 28(4):042101, 2016.

[26] Sally G Harding, David Wessman, Stig Stenström, and Lennart Kenne. Water transport during the drying of cardboard studied by nmr imaging and diffusion techniques. *Chemical engineering science*, 56(18):5269–5281, 2001.

[27] Johannes Leisen, Barry Hojjatie, Douglas W Coffin, Sergiy A Lavrykov, Bandaru V Ramarao, and Haskell W Beckham. Through-plane diffusion of moisture in paper detected by magnetic resonance imaging. *Industrial & engineering chemistry research*, 41(25):6555–6565, 2002.

[28] Jean-Christophe Perrin, Carina Waldner, Julie Bossu, Aninda Chatterjee, and Ulrich Hirn. Real time monitoring of the through thickness moisture profile of thin sheets using nmr. *Chemical Engineering Science*, 251:117464, 2022.

[29] Jonathan M. Schuster, Carlos E. Schvezov, and Mario R. Rosenberger. Influence of experimental variables on the measure of contact angle in metals using the sessile drop method. *Procedia Materials Science*, 8:742–751, 2015. International Congress of Science and Technology of Metallurgy and Materials, SAM - CONAMET 2013.

[30] Maria Ponomar, Ekaterina Krasnyuk, Dmitrii Butylskii, Victor Nikonenko, Yaoming Wang, Chenxiao Jiang, Tongwen Xu, and Natalia Pismenskaya. Sessile drop method: Critical analysis and optimization for measuring the contact angle of an ion-exchange membrane surface. *Membranes 2022, Vol. 12, Page 765*, 12:765, 8 2022.

[31] TAPPI. Water absorptiveness of sized (non-bibulous) paper, paperboard, and corrugated fiberboard (cobb test). *T 441 Om-09*, 2009.

[32] Brian C Smith. *Fundamentals of Fourier transform infrared spectroscopy*. CRC press, 2011.

[33] Stuart Hobson and Niketh Venkatesh. Experimental method development for mri moisture measurements in paper materials. 2022.

[34] Sarah Marie Lößlein, Rolf Merz, Daniel Wyn Müller, Michael Kopnarski, and Frank Mücklich. An in-depth evaluation of sample and measurement induced influences on static contact angle measurements. *Scientific Reports |*, 12:19389, 123.

[35] Chun Haow Kung, Pradeep Kumar Sow, Beniamin Zahiri, and Walter Mérida. Assessment and interpretation of surface wettability based on sessile droplet contact angle measurement: Challenges and opportunities. *Advanced Materials Interfaces*, 6(18):1900839, 2019.

[36] Khaoula Khwaldia. Physical and mechanical properties of hydroxypropyl methylcellulose-coated paper as affected by coating weight and coating composition. *BioResources*, 8(3), 2013.

[37] Masruroh and Dionysius J.D.H. Santjojo. Surface modification of polystyrene by nitrogen plasma treatment. In Jaime Andres Perez-Taborda and Alba G. Avila Bernal, editors, *Coatings and Thin-Film Technologies*, chapter 4. IntechOpen, Rijeka, 2018.

[38] Editors of Encyclopaedia Britannica. Polyethylene. `https://www.britannica.com/science/polyethylene`, May 2023.

[39] Gokhan Acik, Musa Kamaci, and C Elif Cansoy. Superhydrophobic eva copolymer fibers: the impact of chemical composition on wettability and photophysical properties.

[40] Eva hot melt adhesives. `http://www.polymerdatabase.com/Adhesives/EVA%20Adhesives.html`.

A

Appendix A - FTIR Spectra

This chapter presents the FTIR spectra for both sides for all samples.

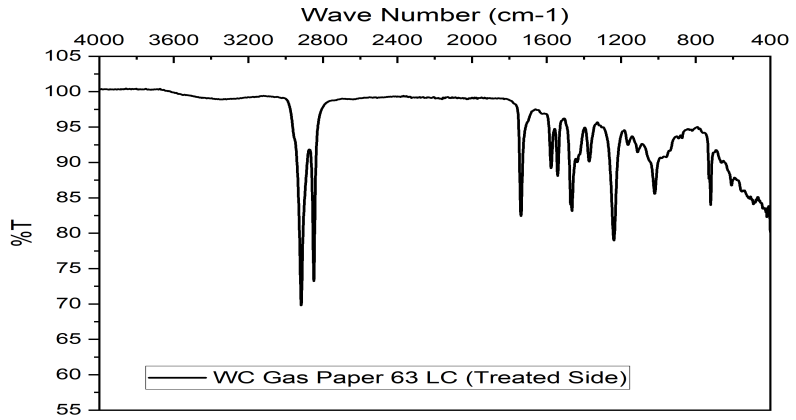

Figure A.1: WC gas paper 63 LC treated side

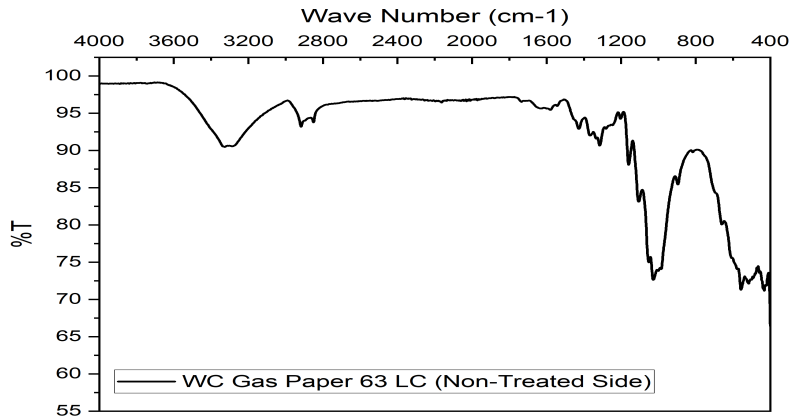

Figure A.2: WC gas paper 63 LC non-treated side

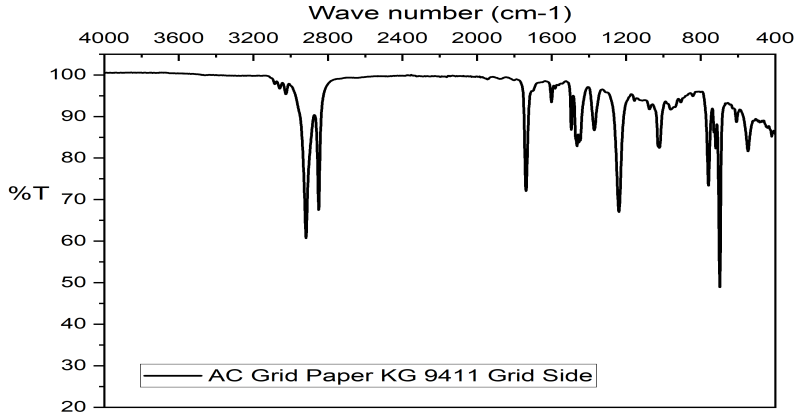

Figure A.3: AC grid paper KG 9411 grid side

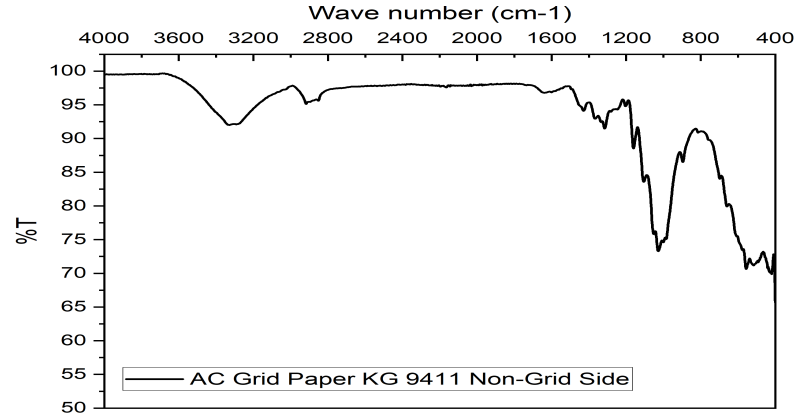

Figure A.4: AC grid paper KG 9411 non-grid side

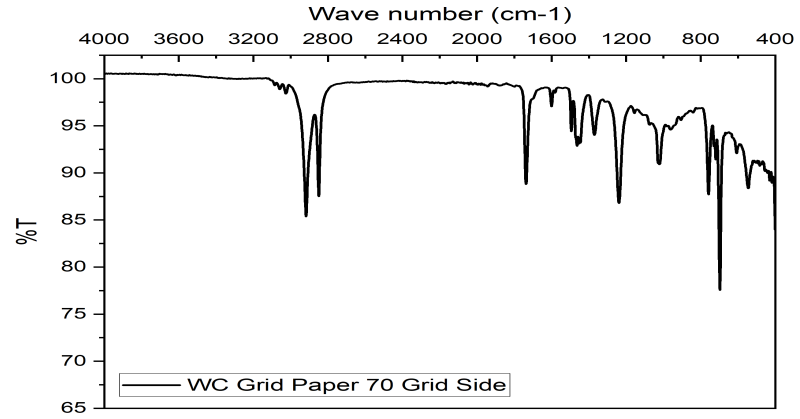

Figure A.5: WC grid paper 70 grid side

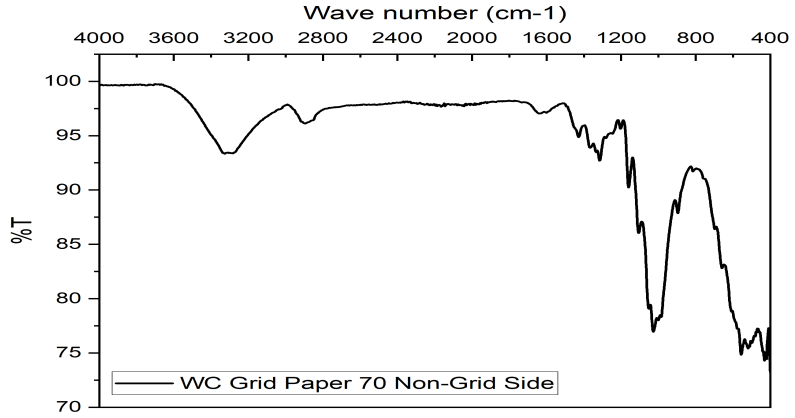

Figure A.6: WC grid paper 70 non-grid side

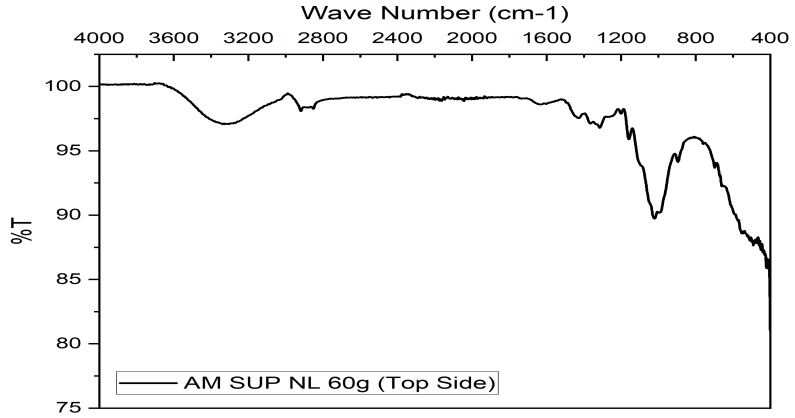

Figure A.7: AM SUP NL 60 g top side

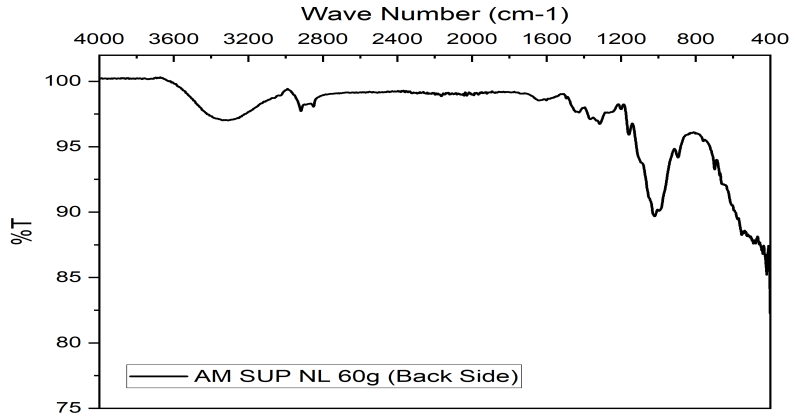

Figure A.8: AM SUP NL 60 g back side

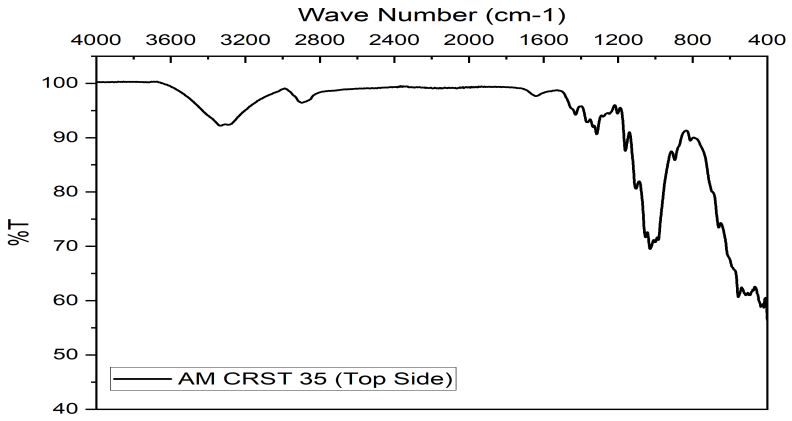

Figure A.9: AM CRSTL 35 top side

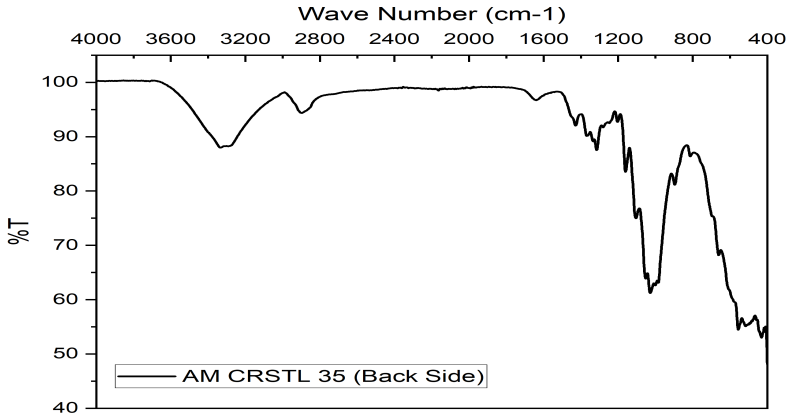

Figure A.10: AM CRSTL 35 back side

B

Appendix B - Contact Angle values

This chapter presents the contact angle values for both sides for all samples.

Table B.1: Water contact angle values of the paper samples (non-treated side)

Sample name	CA(L)	CA(M)	CA(R)
WC gas paper 63 LC	90.69°	90.65°	90.72°
AC grid paper KG 9411	111.68°	111.68°	111.68°
WC grid paper 70	81.53°	82.47°	80.58°
AM SUP NL 60 g	28.35°	28.77°	27.92°
AM CRSTL 35	34.04°	33.61°	34.48°

Table B.2: Salt water contact angle values of the paper samples (non-treated side)

Sample name	CA(L)	CA(M)	CA(R)
WC gas paper 63 LC	110.5°	110.7°	110.9°
AC grid paper KG 9411	120.12°	120.19°	120.26°
WC grid paper 70	84.6°	85.6°	86.5°
AM SUP NL 60 g	44.1°	45.8°	47.58°
AM CRSTL 35	34.3°	35.7°	37.08°

Table B.3: Salt water contact angle values of the paper samples (treated side)

Sample name	CA(L)	CA(M)	CA(R)
WC gas paper 63 LC	112.94°	113.07°	113.20°
AC grid paper KG 9411	88.94°	88.56°	88.19°
WC grid paper 70	86.57°	86.93°	86.565°
AM SUP NL 60 g	45.96°	46.66°	47.37°
AM CRSTL 35	38.24°	38.50°	38.77°

DEPARTMENT Chemistry and Chemical Engineering
CHALMERS UNIVERSITY OF TECHNOLOGY
Gothenburg, Sweden
www.chalmers.se

CHALMERS
UNIVERSITY OF TECHNOLOGY